Lehigh University
Lehigh Preserve

Theses and Dissertations

1989

A light amplification scheme utilizing the nonlinear coherent coupler

Christopher James Milner
Lehigh University

Follow this and additional works at: https://preserve.lehigh.edu/etd

 Part of the Electrical and Computer Engineering Commons

Recommended Citation
Milner, Christopher James, "A light amplification scheme utilizing the nonlinear coherent coupler" (1989). *Theses and Dissertations*. 5231.
https://preserve.lehigh.edu/etd/5231

This Thesis is brought to you for free and open access by Lehigh Preserve. It has been accepted for inclusion in Theses and Dissertations by an authorized administrator of Lehigh Preserve. For more information, please contact preserve@lehigh.edu.

A LIGHT AMPLIFICATION SCHEME

UTILIZING THE NONLINEAR COHERENT COUPLER

by

Christopher James Milner

A Thesis

Présented to the Graduate Committee

of Lehigh University

in Candidacy for the Degree of
Master of Science

in

Electrical Engineering

Lehigh University

1989

Certificate of Approval

This thesis is accepted and approved as partial fulfullment of the requirements of the degree of Master of Science in Electrical Engineering at Lehigh University.

Department Chairman

Advisor

5-19-89

Acknowledgements

The author would like to thank the two individuals in the Computer Science and Electrical Engineering Department who advised him during this thesis project, Nikolai Eberhardt and Demetrios Christodoulides. It was in Dr. Christodoulides' classes that the author was first introduced to the field of integrated optics, and it was Dr. Christodoulides' excellence and enthusiasm in the subject that inspired the author to undertake further study in the field. In Dr. Christodoulides' absence, Dr. Eberhardt provided invaluable guidance and feedback as the thesis was brought together. Without both of these individuals' help, this thesis surely would not have been realized.

The author would also like to thank his family for their continued support throughout this project.

Table of Contents

List of Figures

Abstract

A novel all-optical amplification scheme is proposed using the nonlinear coupler with counter-propagating electromagnetic waves. Amplitude-dependent and phase-independent optical gating has been demonstrated via numerical simulation. Simulations of this three-port device have shown that it can exhibit optical gains on the order of 20 when operated near its inherent instability level.

Chapter 1: Introduction

The following thesis is a report of the work done by Christopher Milner while a Master of Science student at Lehigh University. Along with being a report of the methods, procedures, and results of the simulations conducted, it is intended to provide a relatively comprehensive background on the necessary topics in electromagnetic theory, nonlinear optics, and numerical simulation necessary for completion of this work. The novel optical amplifier discussed in Chapter 3 has, to the extent of the author's knowledge, not been published in the literature. The author intends to pursue publication of these results.

Chapter 2, Background, attempts to provide the reader with the necessary background to fully comprehend the phenomena studied in this paper. It starts with Maxwell's Equations which relate the electric and magnetic fields, and proceeds to present solutions to those equations in waveguiding media. The planar waveguide, circular waveguide, and rectangular waveguide are discussed. A short introduction to nonlinear materials, materials whose effective permitivitty is a function of the electric field strength, is presented. The coupled mode theory, including an introduction to the Lorenz Reciprocity theorem, is presented, with an emphasis on coupling of adjacent waveguides. A brief introduction to the

numerical techniques used in the computer simulations is presented, followed by an introduction to the family of Jacobian elliptic functions, which are used in finding analytic closed-form solutions to the optic couplers discussed.

Chapter 3 discusses the derivation of the equations which describe the operation of the optical amplifier, the numerical techniques used to simulate the optical amplifier, and the results obtained.

Chapter 4 provides a conclusion to the work.

Chapter 2: Background

Section 2.1: Optic Waveguide Theory

Section 2.1.1: Maxwell's Equations

The study of optic waveguide theory involves, at the heart, a study of Maxwell's equations that give the relationship between the electric and magnetic fields. For a dielectric material, these equations take the general form

$$\nabla\times\mathbf{E} = -\frac{\delta}{\delta t}\mathbf{B} \qquad (2.1.1\text{-}1)$$

$$\nabla\times\mathbf{H} = \frac{\delta}{\delta t}\mathbf{D} + \mathbf{J} \qquad (2.1.1\text{-}2)$$

$$\nabla\cdot\mathbf{D} = p \qquad (2.1.1\text{-}3)$$

$$\nabla\cdot\mathbf{B} = 0 \qquad (2.1.1\text{-}4)$$

where $\mathbf{E}(\mathbf{r},t)$ is the electric field as a function of position and time, $\mathbf{H}(\mathbf{r},t)$ is the magnetic field,

$$\mathbf{D}(\mathbf{r},t)=\epsilon\mathbf{E}(\mathbf{r},t) \qquad (2.1.1\text{-}5)$$

is the electric displacement and

$$\mathbf{B}(\mathbf{r},t)=\mu\mathbf{H}(\mathbf{r},t) \qquad (2.1.1\text{-}6)$$

is the magnetic displacement. $\mathbf{J}(\mathbf{r},t)$ and $p(\mathbf{r},t)$ represent any current and charge sources present. The parameter ϵ is the permittivity (or dielectric constant), and in free space $\epsilon=\epsilon_0\approx 8.85\text{X}10^{-12}$ farads/meter (F/m). μ is the permeability of the medium, and in free space, $\mu=\mu_0\approx 4\pi\text{X}10^{-7}$ Henrys/meter (H/m).

2.1.1: Maxwell's Equations

To simplify analysis, we will assume that we are analyzing waves propagating in materials that are linear, so that ϵ and μ are independent of **E** and **B**. We will also assume that the materials are homogeneous, so that ϵ and μ are independent of the position vector **r**, and assume that the materials are isotropic, which means that ϵ and μ are simply scalars, not tensors (the permitivitty and permeability are not functions of direction of travel of electromagnetic radiation). Finally, we assume that there are no current or charge sources present, so **J** and p are zero. Waveguides do not fit this restriction, because they are non-homogenous (their index of refraction varies with position).

If we take the curl of equation (2.1.1-1), and use the vector identity

$$\nabla\times\nabla\times\mathbf{A} = \nabla(\nabla\cdot\mathbf{A}) - \nabla^2\mathbf{A}$$

we get

$$\nabla\times\nabla\times\mathbf{E} = -\frac{\delta}{\delta t}(\nabla\times\mathbf{B}) = \nabla(\nabla\cdot\mathbf{E}) - \nabla^2\mathbf{E}.$$

Since p is zero, then equation (2.1.1-3) tells us that $\nabla\cdot\mathbf{D}$ is zero, and equation (2.1.1-5) tells us that $\nabla\cdot\mathbf{E}$ is zero, which leads us to Maxwell's wave equation,

$$\nabla^2\mathbf{E} - \mu_0\mu_r\epsilon_0\epsilon_r\frac{\delta^2}{\delta t^2}\mathbf{E} = 0 \qquad (2.1.1\text{-}7)$$

If we define $v=(\mu_0\mu_r\epsilon_0\epsilon_r)^{-\frac{1}{2}}$, then Maxwell's wave equation has solutions

$$\mathbf{E} = \mathbf{E}_1(\mathbf{r}\pm vt).$$

2.1.1: Maxwell's Equations

In most dielectrics $\mu_r = 1$, so that $v=c(\epsilon_r)^{-\frac{1}{2}}$, where $c=(\mu_0\epsilon_0)^{-\frac{1}{2}}$ is the velocity of light in free space, and $(\epsilon_r)^{\frac{1}{2}} = c/v = n$, the index of refraction. This leads to another useful form of Maxwell's wave equation,

$$\nabla^2\mathbf{E} - \frac{n^2(\mathbf{r})}{c^2}\frac{\delta^2}{\delta t^2}\mathbf{E} = 0 \qquad (2.1.1\text{-}8)$$

If we consider time harmonic fields, with $\mathbf{E}(\mathbf{r},t)=\mathbf{E}(\mathbf{r})e^{-j\omega t}$, and inserting this into equation (2.1.1-8), we see that

$$\nabla^2\mathbf{E} + \frac{\omega^2 n^2}{c^2}\mathbf{E} = 0 \qquad (2.1.1\text{-}9)$$

which is the Helmholz equation in vector form. The vector quantity **E** can be broken down into its x, y, and z components, and the Helmholz equation holds true for each component. For example, let $E_x = E_{x0}e^{j(k_x x + k_y y + k_z z)} = E_{x0}e^{j\mathbf{kr}}$, and plug this into equation (2.1.1-9), then $-(k_x^2+k_y^2+k_z^2)+k^2 = 0$, where $k^2 = \frac{\omega^2 n^2}{c^2}$. We can see that the wave travels along the k vector.

Waveguide Equations - Infinite Planar Waveguides

The phenomenon of guided (electromagnetic) waves occurs when waves are propagating in media with inhomogeneous indices of refraction. Solutions of Maxwell's equations, together with boundary conditions induced where the index of refraction

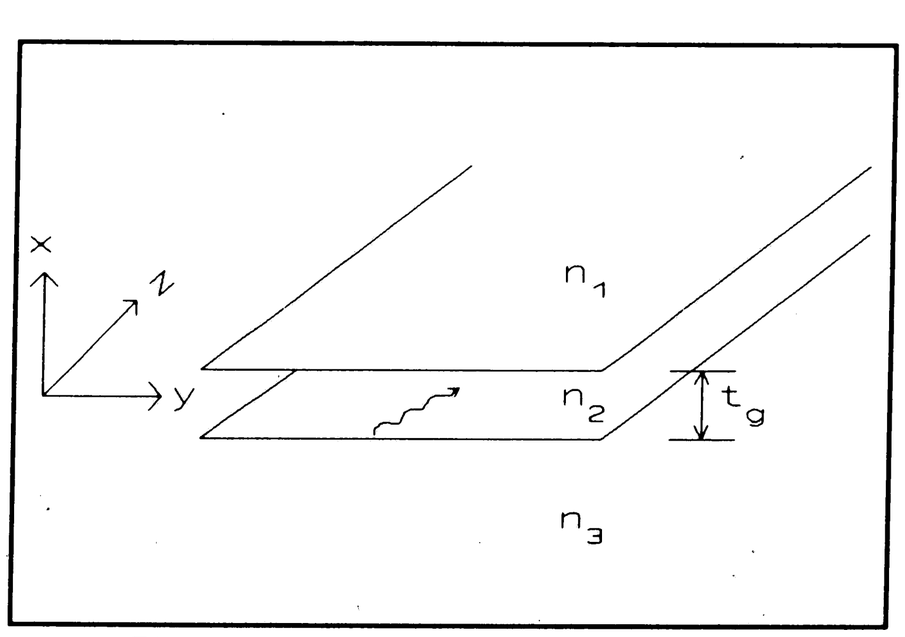

Figure 1: Infinite Planar Waveguide

changes, describe propagation of guided and evanescent propagating waves. Assume an infinite dielectric planar waveguide as shown in Figure 1, with the structure infinitely large in the y and z directions. Assume that in region 1, above the waveguide, the material has index of refraction n_1, and in regions 2 and 3, respectively, the material has indices of refraction n_2 and n_3. As we will see, for waveguiding to occur, n_2 will have to be greater that n_1 and n_3. Any electric field propagating in this medium must satisfy Maxwell's wave equation, here used in the form of equation (2.1.1-9). Let us consider first a simple case in which the electric field **E** lies in the x-y plane. Such a field is denoted transverse electric with respect to z, or TE_z. We will place the further restriction that the electric field be parallel to the y axis, and is constant with respect to y. Then the Laplacian operator reduces to a much simpler operation, since $\frac{\delta}{\delta y}\mathbf{E}=0$. The associated magnetic components will consist of an H_x and an H_z component. Plugging the solution $\mathbf{E}(\mathbf{r},t)=\mathbf{E}(x,y)e^{j(\omega t-\beta z)}$ into the wave equation, and noting that the ∇^2 operator becomes $\delta_{xx}+\delta_{zz}$, we have,

$$\begin{aligned} &\text{Region 1:} \quad \frac{\delta^2}{\delta x^2}\mathbf{E}+(k_0^2n_1^2-\beta^2)\mathbf{E}=0 \\ &\text{Region 2:} \quad \frac{\delta^2}{\delta x^2}\mathbf{E}+(k_0^2n_2^2-\beta^2)\mathbf{E}=0 \qquad (2.1.1\text{-}10) \\ &\text{Region 3:} \quad \frac{\delta^2}{\delta x^2}\mathbf{E}+(k_0^2n_3^2-\beta^2)\mathbf{E}=0 \end{aligned}$$

For the wave to be guided, the fields outside of the waveguide, in regions 1 and 3, must decay. This means that

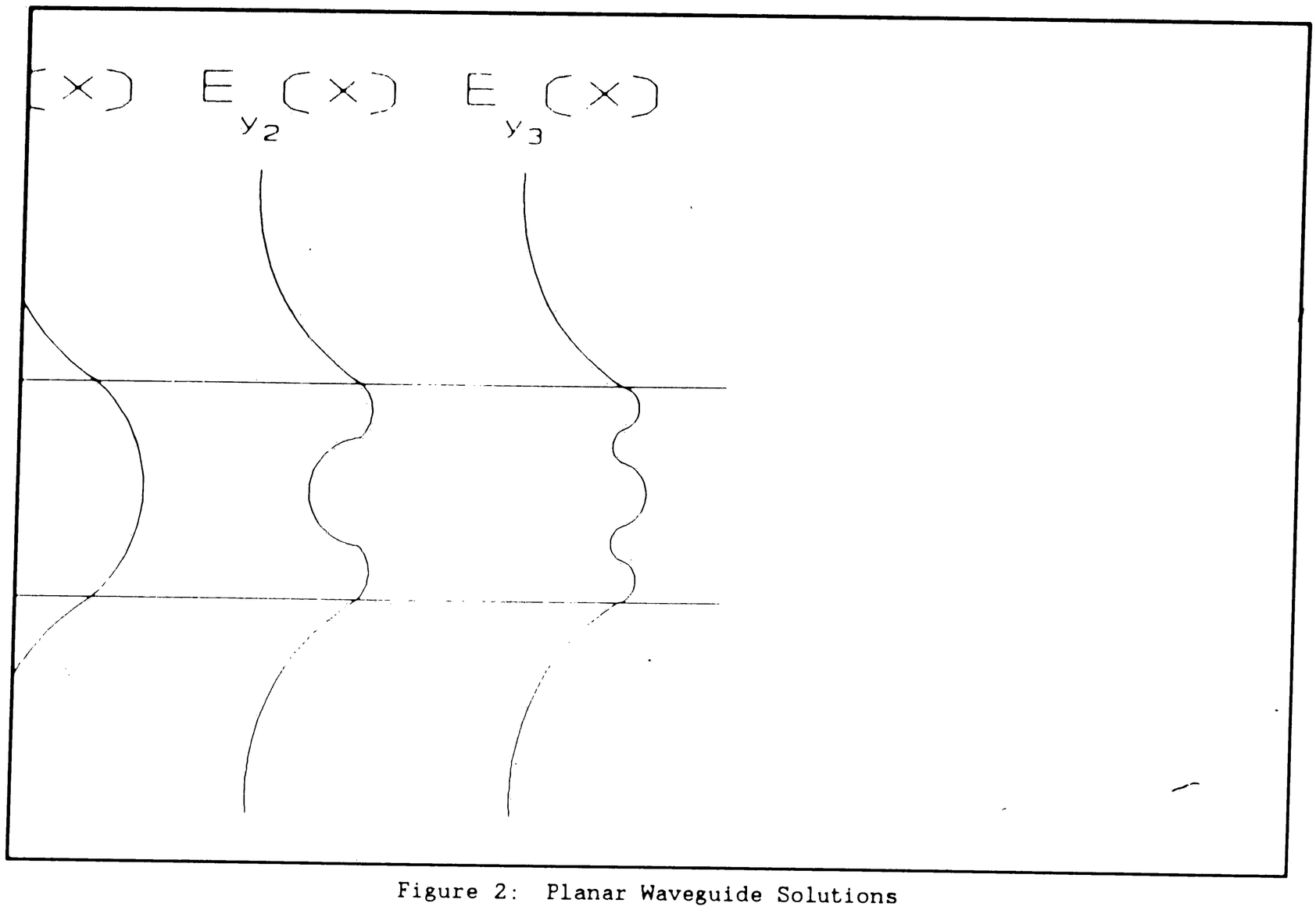

Figure 2: Planar Waveguide Solutions

in region 1, $\beta>k_0n_1$, and in region 3, $\beta>k_0n_3$. In region 2, $\beta<k_0n_2$ admits solutions sinusoidal with x, as depicted in Figure 2. We see that waveguiding occurs when a 'channel', or guide, exists with higher index of refraction than the surrounding indices of refraction. Expressed in terms of n_1, n_2, and n_3, the following 2 relations must hold:

$$n_2>n_1 \text{ and } n_2>n_3.$$

The degree to which n_2 is greater than n_1 and n_3 determines which frequencies, or modes, of waves which will be guided and which will not be guided. The smaller of the two differences (n_2-n_3) and (n_2-n_1) will determine the cutoff conditions. It can be shown ([1], chapter 3) that by solving

equations (2.1.1-10) with requirements that E_y be continuous and that the derivative of E_y be continuous at every interface, a set of discrete allowed values of β exist, described by the transcendental equation

$$\tan(ht_g)=\frac{(p+q)h}{(h^2-pq)} \qquad (2.1.1\text{-}11)$$

where

$$q=(\beta^2-n_1^2k^2)^{\frac{1}{2}},$$

$$h=(n_2^2k^2-\beta^2)^{\frac{1}{2}},$$

$$q=(\beta^2-n_3^2k^2)^{\frac{1}{2}},$$

$$k=\omega/c, \qquad (2.1.1\text{-}12)$$

and t_g is the thickness of the waveguide, as shown in Figure 1.

We next consider the case of the waveguide discussed above, where symmetry in the y direction exists, i.e., $n_1=n_3$. The cutoff condition for propagation of a wave with propagation constant β will be when

$$\beta=kn_1=kn_3. \qquad (2.1.1\text{-}13)$$

substituting into (2-8) to find q, h, and p, and further substituting into (2-7) to find allowable values for ht_g, we come to the condition of guiding for mode m_s

$$\Delta n=(n_2-n_1)>\frac{m_s^2\lambda_0^2}{4t_g^2(n_2+n_1)},\ m_s=0,\ 1,\ 2,\ 3,\ \ldots \qquad (2.1.1\text{-}14)$$

The cutoff condition given in (2.1.1-14) defines which modes are supported by a planar waveguide given a particular λ_0, Δn, and t_g. It is interesting to note that the zeroth mode ($m_s=0$) has no cutoff in a symmetric waveguide, and will always

propagate, although confinement may be low, and the attenuation of a poorly guided mode is high.

The asymmetric waveguide, with $n_1 \ll n_3$, but n_2 still greater than n_3, is interesting in that the zeroth mode does not always propagate. The waveguiding condition for the m^{th} mode is ([2], p.37)

$$\Delta n = (n_2 - n_3) > \frac{(2m+1)^2 \lambda_0^2}{16 t_g^2 (n_2 + n_3)}, \quad m = 0, 1, 2, 3 \ldots \quad (2.1.1\text{-}15)$$

By changing the index of refraction n_3 from n_1 to a value greater than n_1 but still less than n_2, it is possible to prevent the zeroth mode from propagating[36]. This phenomenon has applications in optical switching. When n_3 can be changed by an external electrical or optical signal via the electrooptic effect, propagation of light in the waveguide can be controlled.

In any waveguide with at least two modes propagating, it will be shown that any pair of modes is mutually orthogonal. This fact will be used later in this thesis when coupled mode theory is developed, but is presented here to maintain contextual integrity. Consider two guided modes TE_m and TE_j, with respective propagation constants β_m and β_j. Both of these modes will satisfy the wave equation, and both of these modes and their derivatives will decay to zero as x approaches infinity. If we take the two equations

$$\ddot{E}_m + (k_0^2 n^2(x) - \beta_m^2) E_m = 0$$
$$\ddot{E}_j + (k_0^2 n^2(x) - \beta_j^2) E_j = 0 \quad (2.1.1\text{-}16)$$

and multiply the top equation by E_j and the bottom equation by $-E_m$ and add them, we have

$$(\ddot{E}_m E_j - E_m \ddot{E}_j) = (\beta_m^2 - \beta_j^2) E_m E_j \qquad (2.1.1\text{-}17)$$

and integrating from $x=-\infty$ to $x=\infty$, with some manipulation we see that

$$\int_{-\infty}^{\infty} dx E_m E_j = \delta_{jm} \qquad (2.1.1\text{-}18)$$

which may be interpreted as evidence that any two modes with non-equal propagation constants are orthogonal.

A parallel derivation of the mode guiding conditions may be developed for waves with only one magnetic field component, H_y, and two electric field components, E_x and E_z. A wave equation for the magnetic field may be developed from equations (2.1.1-1) in the same manner as for the electric field, and solutions for the wave equation within planar waveguides may be calculated. This family of modes is known as TM modes.

Section 2.1.2: Circular Waveguides

To attain a detailed understanding of the optical power propagation in an optical fiber, Maxwell's equations must be solved subject to the cylindrical boundary conditions of the fiber. We will be considering electromagnetic waves propagating in a cylindrical coordinate system with a cylindrical boundary, as shown in Figure 3. If the

2.1.2: Circular Waveguides

electromagnetic waves are to propagate along the z axis, the electric and magnetic fields will in general have the functional dependence of the form

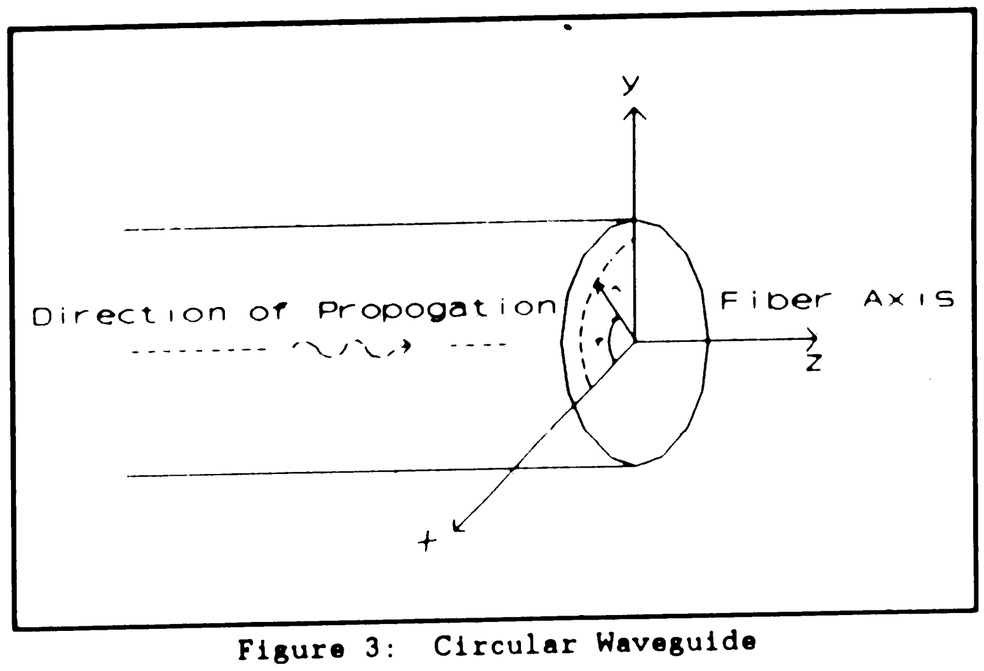

Figure 3: Circular Waveguide

$$\mathbf{E}=\mathbf{E}_0(r,\phi)\,e^{j(\omega t-\beta z)} \qquad (2.1.2\text{-}1)$$

$$\mathbf{H}=\mathbf{H}_0(r,\phi)\,e^{j(\omega t-\beta z)} \qquad (2.1.2\text{-}2)$$

As in the planar waveguide, the parameter β is the propagation constant which will be determined by the boundary conditions. When equations (2.1.2-1) and (2.1.2-2) are substituted into Maxwell's curl equation in cylindrical coordinates, we may derive the wave equations in cylindrical coordinates, ([1], p.29)

$$\frac{\delta^2}{\delta r^2}\mathbf{E}_z + \frac{1}{r}\frac{\delta}{\delta r}\mathbf{E}_z + \frac{1}{r^2}\frac{\delta^2}{\delta \phi^2}\mathbf{E}_z + q^2\mathbf{E}_z = 0 \qquad (2.1.2\text{-}3)$$

$$\frac{\delta^2}{\delta r^2}\mathbf{H}_z + \frac{1}{r}\frac{\delta}{\delta r}\mathbf{H}_z + \frac{1}{r^2}\frac{\delta^2}{\delta \phi^2}\mathbf{H}_z + q^2\mathbf{H}_z = 0 \qquad (2.1.2\text{-}4)$$

where $q^2=\omega^2\epsilon\mu-\beta^2 = k^2 - \beta^2$. These equations are the cylindrical counterparts to the wave equations developed in §2.1.1 for planar waveguides. It will be possible to generate TE modes, in which $E_z=0$, and TM modes, in which $H_z=0$, and also hybrid

modes, in which neither E_z or H_z are zero. In this way, the analysis of optical fibers is more complicated than hollow metal tube waveguides in which only TE and TM modes are found.

To solve for the fields given certain boundary conditions, the standard technique of separation of variables is used. For a transverse electric (TE) mode, the solution of equation (2.1.2-3) is assumed to be of the form

$$E_z = C \cdot F_r(r) \cdot F_\phi(\phi) \cdot F_z(z) \cdot F_t(t) \qquad (2.1.2\text{-}5)$$

where, since we are assuming solutions of the form described in (2.1.2-1),

$$F_z(z) \cdot F_t(t) = e^{j(\omega t - \beta z)} \qquad (2.1.2\text{-}6)$$

and because of the circular symmetry of the waveguide, $F_\phi(\phi)$ must have periodicity of 2π, or

$$F_\phi(\phi) = e^{j\eta\phi} \qquad (2.1.2\text{-}7)$$

where η is an integer, positive or negative. The only remaining component of E_z to be determined is the radial component, $F_r(r)$. Substituting (2.1.2-7) and (2.1.2-6) into (2.1.2-5), the wave equation for F_r becomes

$$\frac{\delta^2}{\delta r^2}F_r + \frac{1}{r}\frac{\delta}{\delta r}F_r' + \left\{q^2 - \frac{\eta^2}{r^2}\right\}F_r = 0 \qquad (2.1.2\text{-}8)$$

which is a well-known differential equation for Bessel functions. An identical equation for $H_r(r)$ may be developed.

For the configuration of a step-index fiber we consider a circular dielectric waveguide with index of refraction n_1 for $0 \le r \le r_{core}$, and n_2 for $r_{core} < r < \infty$ (see Figure 4). The region outside of the core is known as the cladding, and for

simplicity of calculation we assume it to be infinitely large. This is allowable because the fields outside of the core decay exponentially, and in actual fibers the cladding is of sufficient

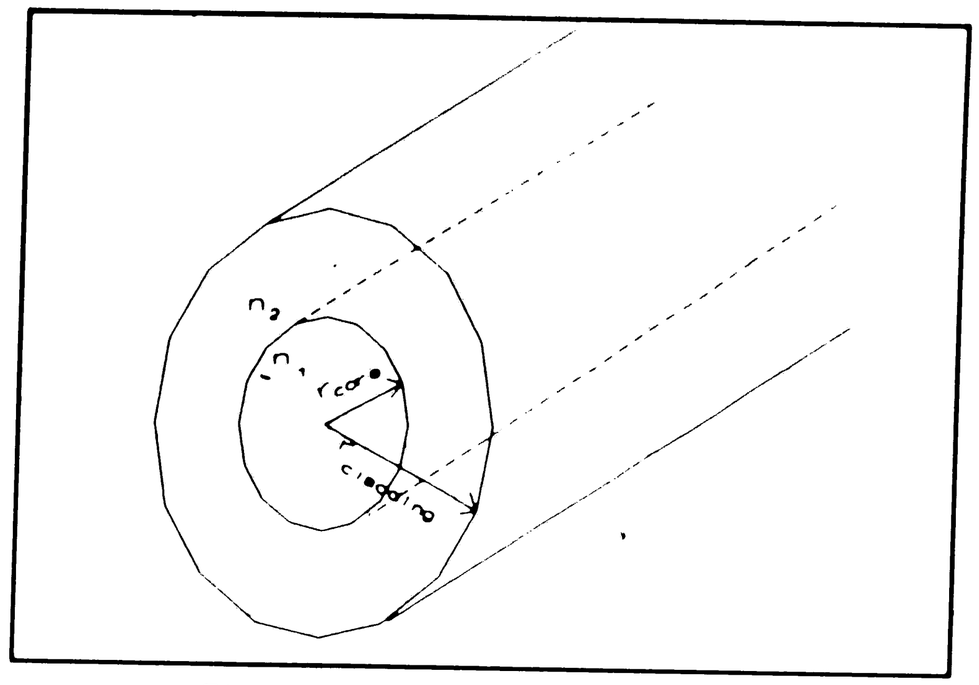

Figure 4: Optic Fiber Waveguide

diameter to make the fields at the outer edge of the cladding negligible. The field patterns, or modes, in a circular waveguide are similar to those in the infinite planar waveguide, with the r dimension corresponding to the y dimension. Equation (2.1.2-8) must now be solved for the core region and the cladding region. In the core region, the solutions to (2.1.2-8) must be finite at r=0, and are given in terms of the modified Bessel functions of the first kind of order η $J_\eta(r)$, and in the cladding, the solutions must approach zero as r approaches ∞, and are given in terms of the modified Bessel functions of the second kind of order η, $K_\eta(r)$. Therefore, for a given r_{core}, and a given n_{core} and $n_{cladding}$, we have

$$E(0\le r\le r_{core}) = AJ_\eta(ur)\,e^{j\eta\phi}e^{j(\omega t-\beta z)} \qquad (2.1.2\text{-}9)$$

$$H(0\le r\le r_{core}) = BJ_\eta(ur)\,e^{j\eta\phi}e^{j(\omega t-\beta z)} \qquad (2.1.2\text{-}10)$$

$$E(r_{core}\le r<\infty) = CK_\eta(wr)\,e^{j\eta\phi}e^{j(\omega t-\beta z)} \qquad (2.1.2\text{-}11)$$

$$H(r_{core}\le r<\infty) = DK_\eta(wr)\,e^{j\eta\phi}e^{j(\omega t-\beta z)} \qquad (2.1.2\text{-}12)$$

where A, B, C, and D are arbitrary constants, and $u^2=k_1^2-\beta^2$, $w^2=\beta^2-k_2^2$, $k_1=2\pi n_{core}/\lambda_0$, and $k_2=2\pi n_{cladding}/\lambda_0$. From the definition of the Bessel functions, we see that $K_\eta(wr)\rightarrow e^{-wr}$ as $wr\rightarrow\infty$. For $K_\eta(wr)$ to go to zero as r goes to infinity, w must be greater than zero, which in turn implies that in the cladding, $\beta\geq k_2$. In the core, the parameter u must be real for $F_r(r)$ to be real, which leads to the condition than in the core, $\beta\leq k_1$. The allowable range of β for guided modes is therefore

$$2\pi n_{cladding}/\lambda_0 \leq \beta \leq 2\pi n_{core}/\lambda_0 \qquad (2.1.2\text{-}13)$$

with particular values of β determined from the boundary conditions. If we require that the tangential components of E_z and H_z be continuous at the core-cladding boundary, then the following eigenvalue equation for β results (after considerable manipulation) ([1], p.33)

$$\left\{\frac{J'_\eta(ur_{core})}{uJ_\eta(ur_{core})}+\frac{K'_\eta(wr_{core})}{wK_\eta(wr_{core})}\right\}\left\{k_1^2\,\frac{J'_\eta(ur_{core})}{uJ_\eta(ur_{core})}+k_2^2\,\frac{K'_\eta(wr_{core})}{wK_\eta(wr_{core})}\right\}=\left\{\frac{\beta\eta(u^2+w^2)}{r_{core}u^2w^2}\right\}^2 \qquad (2.1.2\text{-}14)$$

which is a complicated transcendental equation to give the discrete allowable values of β, within the range specified by (2.1.2-13), for a step-index fiber.

An important quantity related to the mode cutoff conditions is the normalized frequency V, or V-number, defined by

$$V^2 = (u^2 + w^2)r_{core}^2 = \left\{\frac{2\pi r_{core}}{\lambda}\right\}^2(n_{core}^2 - n_{cladding}^2) \qquad (2.1.2\text{-}15)$$

2.1.2: Circular Waveguides

The number of modes b that can exist in a fiber as a function of V may be represented by

$$b = \frac{r_{core}^2 w^2}{V^2} = \frac{(\beta/k)^2 - n_{cladding}^2}{n_{core}^2 - n_{cladding}^2} \qquad (2.1.2\text{-}16)$$

A plot of b as a function of V is shown in Figure 5 for a few values of the low order modes. From the figure it can be seen that the lowest order mode, a hybrid HE_{11} mode, has no cutoff condition, and always propagates. This phenomenon is used to create single-mode fibers, by letting the dimensions of the core be small (10λ) and having small index of refraction differences between the core and the cladding. Fibers with Δn on the order of .001, or 0.1%, are commonly used as single-mode fibers[1].

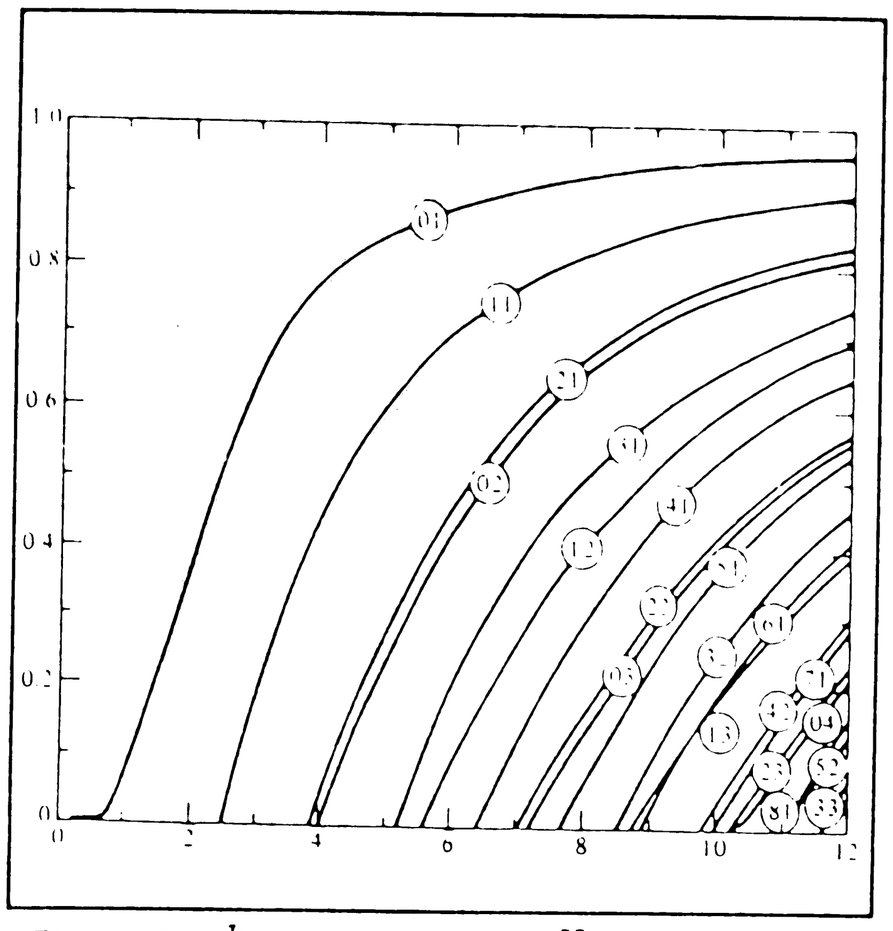

Figure 5: b as a Function of V for some lower order modes

As with planar waveguides, mode orthogonality relations exist. In an optical fiber with multiple modes propagating, the relationship

$$\int_{r=-\infty}^{\infty}\int_{\phi=0}^{2\pi} dA\ E_m E_n = \delta_{mn} \qquad (2.1.2\text{-}17)$$

holds.

2.1.2: Circular Waveguides

Section 2.1.3: Rectangular Dielectric Waveguides

The analysis of rectangular dielectric waveguide is similar to the previous analyses of planar and circular waveguides in that Maxwell's equations must once again be solved subject to the boundary condition constraints introduced by the geometry of the waveguide. The solutions will be oscillatory within the waveguide and exponentially decreasing outside of the waveguide.

The general rectangular dielectric waveguide consists of a guiding region of index n_1 surrounded on all sides by regions with (lesser) indices n_2, n_3, n_4, etc (see Figure 6). Although the exact solution of the wave equation for the entirely asymmetric channel waveguide in Figure 6 is as yet unknown ([2], p.38), we can make approximations when symmetry exists. Separation of variables allows us to consider the E_y (or H_x) as a function of y separately from E_y (or H_x) as a function of x (see Figure 6). The solutions of the separate components are the same as the solutions observed earlier for planar waveguides, and the product $E_y(x) \cdot E_y(y)$ determines the electric field $E_y(x,y)$. The resulting field is denoted E^a_{nm}, where a is the axis to which

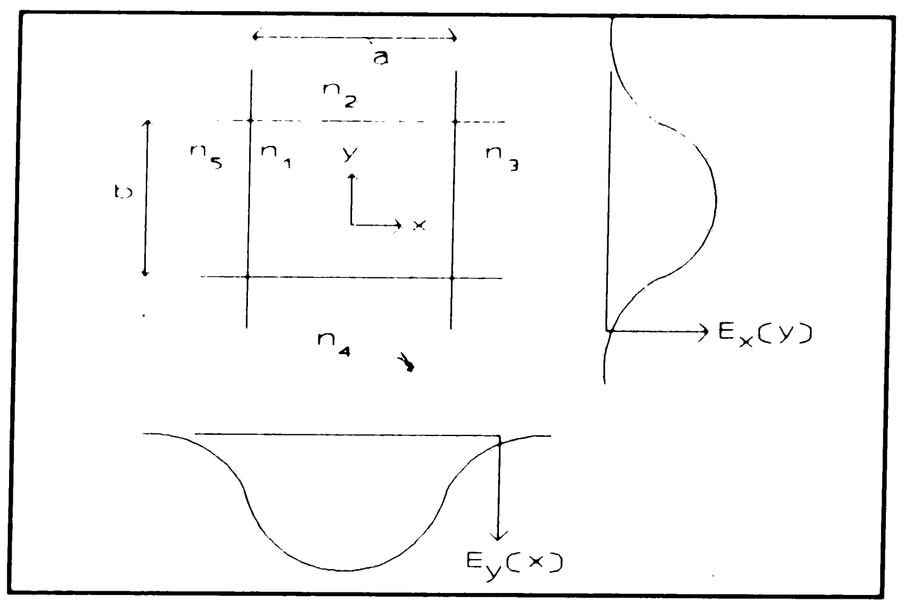

Figure 6: General Channel Dielectric Waveguide

the field is parallel, n is the number of field maxima along the x axis, and m is the number of field maxima along the y axis.

Fabrication of a perfectly symmetric channel waveguide is prohibitively impractical. The channel waveguides commonly fabricated are strip-loaded waveguides, where an effective channel is induced in a thin film by a strip of material applied on top of the thin film which produces an effective index change. As is illustrated in Figure 7, a thin film of index of refraction n_1 is induced upon a substrate of (lesser) index of refraction n_2. Then a waveguiding channel is created in the thin film either by deposition of a dielectric strip or metal strips on top of the thin film[2]. In the former case, a dielectric of lesser index of refraction than the thin film is deposited directly over the desired waveguiding channel (Figure 7(a)), and this induces a local effective increase in the index of refraction in the channel region, therefore providing waveguiding. In the case of metallic loading strips being used to produce

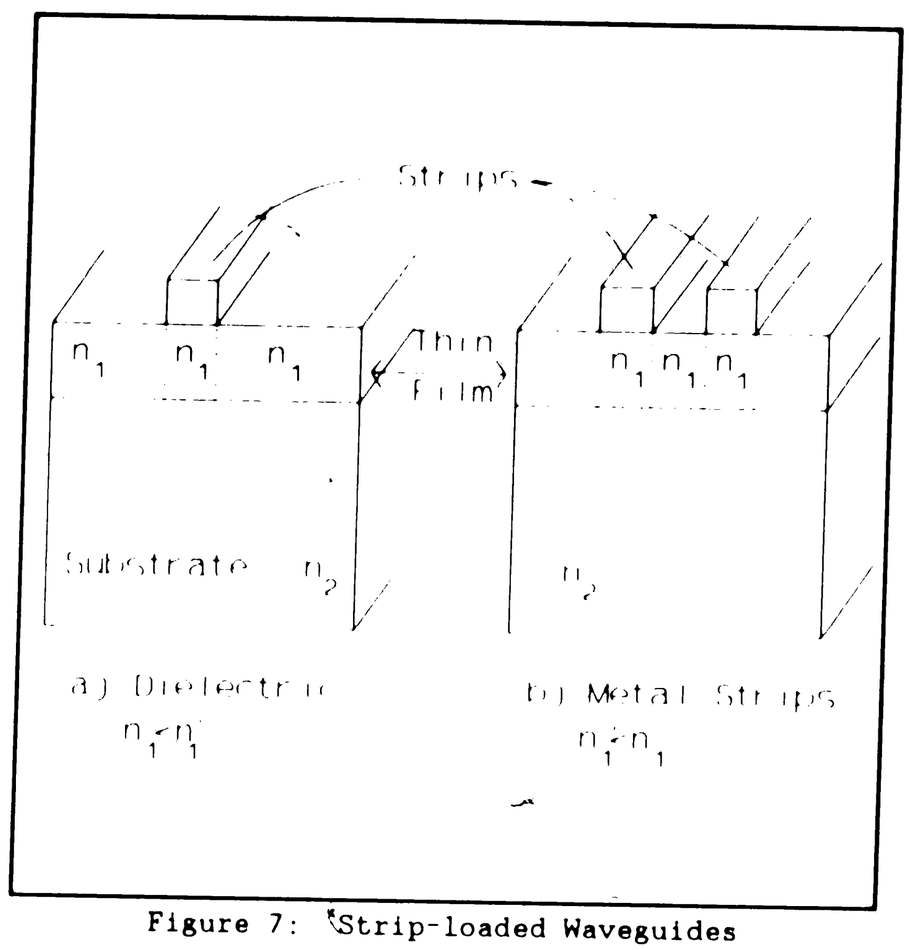

Figure 7: Strip-loaded Waveguides

waveguiding channels (see Figure 7(b)), two metal loading strips are placed upon the surface of the waveguiding layer on either side of the region in which confinement is desired producing effective index reductions, and providing waveguiding in the center region. Since in both cases, the index difference between the channel and the substrate is much larger than between the channel and the surrounding thin film, the cutoff condition for waveguiding will be determined by $\Delta n=(n_1 - n_1')$.

Section 2.1.4: Nonlinear Materials

For this thesis the type of non-linear materials considered have indices of refraction which can be written in the form $n = n_0 + n_2 I$, where n_0 is the linear component of the index, and n_2 is the nonlinear coefficient sometimes referred to as the self-focusing coefficient, and I is the optical power density. (The factor n_1 is generally reserved to show any position-depend inhomogeneities of the material, for instance in

Material	n	$n_2(m^2/W)$
CS_2	1.61	3.0×10^{-18}
SF-59	1.91	6.8×10^{-19}
SF-58	1.88	4.9×10^{-19}
SF-57	1.81	4.1×10^{-19}
SF-56	1.75	2.6×10^{-19}
FDS-90	1.81	2.2×10^{-19}
FDS-9	1.81	1.2×10^{-19}
FD-60	1.77	2.0×10^{-19}
FD-6	1.77	1.7×10^{-19}
E-1	1.93	4.9×10^{-19}
Rutile	2.48	2.0×10^{-18}

Figure 8: Measured Values of n_2

periodic Bragg structures.) The coefficient n_2, also sometimes known as the Kerr coefficient, is typically very much smaller than n_0. The largest values of n_2 are found in certain types of glasses, and actual values for n_2 have been well-researched in the literature[3,4]. The exact cause of power-dependent changes in the index of refraction is unknown, but it is believed to arise primarily from electronic effects, and has response (and relaxation) times which have been measured to be faster than 100fs[4]. Figure 8, taken from [3], shows values of n_2 for certain materials at $\lambda = 1.06\mu m$.

Section 2.1.5: Coupled Mode Theory

When two or more waveguides are placed in proximity to each other, such that the evanescent fields outside of the waveguides overlap, there is a power exchange between them, the amount of exchange being determined primarily by the closeness and similarity of the waveguides. This is known as waveguide coupling, and a device in which coupling occurs is known as a coupler, or directional coupler. If the materials from which the coupler is made have nonlinearities, there are certain nonlinear effects, and the device is known as a nonlinear coupler. Mode coupling can happen between different modes in a single waveguide, and can even happen between modes propagating in opposite directions in a waveguide, as found

in a device known as a grating reflector. The mathematics that describe the coupling phenomenon are called coupled mode theory, and are presented here, with a particular emphasis on the directional coupler.

Many times is it necessary to analyze the optical properties of waveguides that are too complicated to be conveniently solved by either the ray optic approach or by rigorous application of Maxwell's equations. However, many of these problems may be considered as perturbations of simpler problems which have already been solved, or are simple enough to solve. To relate the perturbed case to the unperturbed case, the Lorenz reciprocity theorem is used. In the case of mode coupling between two parallel and identical waveguides, the modes of each individual waveguide are considered separately. Then it is assumed that all modes of the coupled system can be represented as linear combinations of the perturbed modes of the uncoupled systems. This is the key concept behind coupled mode theory.

The Lorenz Reciprocity Theorem

Consider one waveguide, with **E** and **H** being valid solutions to Maxwell's wave equation within the waveguide which has permittivity $\epsilon(x,y,z)$, as discussed in §2.1.1. Assume that the perturbed system (in this case, a two-

waveguide system) has permitivitty $\epsilon'(x,y,z)$, with associated valid solutions $\mathbf{E}'$ and $\mathbf{H}'$ (see Figure 5). Then Maxwell's wave equations for the two cases are:

$$\begin{aligned} &\text{Perturbed:} && 1)\ \nabla\times\mathbf{E} = -j\omega\mu\mathbf{H} \\ &&& 2)\ \nabla\times\mathbf{H} = j\omega\epsilon\mathbf{E} \\ &\text{Unperturbed:} && 3)\ \nabla\times\mathbf{E}' = -j\omega\mu\mathbf{H}' \\ &&& 4)\ \nabla\times\mathbf{H}' = j\omega\epsilon'\mathbf{E}'. \end{aligned} \qquad (2.1.5\text{-}1)$$

Now, taking the quantity

$$\mathbf{E}^*\cdot(4) - \mathbf{H}'\cdot(1)^* - \mathbf{H}^*\cdot(3) + \mathbf{E}'\cdot(2)^* = 0,$$

we see that

$$(\mathbf{E}^*\cdot\nabla\times\mathbf{H}' - \mathbf{H}'\cdot\nabla\times\mathbf{E}^*) - (\mathbf{H}^*\cdot\nabla\times\mathbf{E}' - \mathbf{E}'\cdot\nabla\times\mathbf{H}^*) = +j\omega(\epsilon'-\epsilon)\mathbf{E}^*\cdot\mathbf{E}'.$$

Then we use the vector identity

$$\nabla\times(\mathbf{A}\times\mathbf{B}) = \mathbf{B}\cdot\nabla\times\mathbf{A} - \mathbf{A}\cdot\nabla\times\mathbf{B}$$

and we see

$$-\nabla\times(\mathbf{E}^*\times\mathbf{H}') + \nabla\times(\mathbf{H}^*\times\mathbf{E}') = j\omega(\epsilon'-\epsilon)\mathbf{E}^*\cdot\mathbf{E}'$$

which further simplifies to

$$\nabla\times(\mathbf{E}^*\times\mathbf{H}' - \mathbf{H}^*\times\mathbf{E}') = -j\omega(\epsilon' - \epsilon)\mathbf{E}^*\cdot\mathbf{E}'. \qquad (2.1.5\text{-}2)$$

We then use Gauss' theorem and integrate both sides of this equation over a volume V, to yield

$$\iint_S (\mathbf{E}^*\times\mathbf{H}' + \mathbf{E}'\times\mathbf{H}^*)\cdot d\mathbf{S} = -j\omega\iiint_V (\epsilon - \epsilon')\mathbf{E}^*\cdot\mathbf{E}'\ dV \qquad (2.1.5\text{-}3)$$

which is the Lorenz reciprocity theorem. We will now derive a special case for the Lorenz Reciprocity Theorem for the general class of cylindrically symmetric waveguides, and relate the results to coupled mode theory.

2.1.5: Coupled Mode Theory

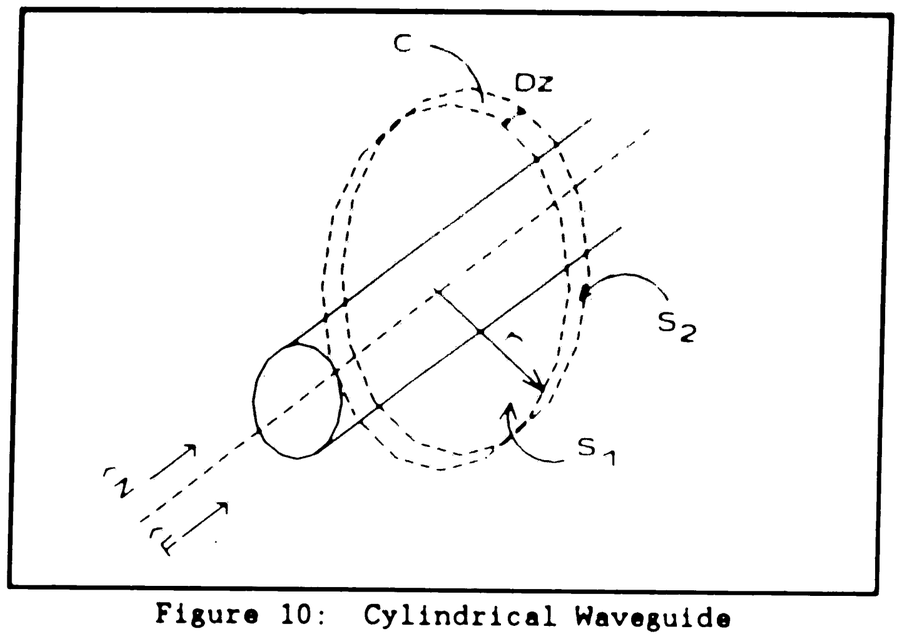

Figure 10: Cylindrical Waveguide

Consider a cylindrical (or any radially symmetric) waveguide with an electromagnetic field propagating along it, as shown in Figure 10. Since we are free to choose any closed surface when performing the integrals above, choose the surface shown in Figure 10, with two circular sides S_1 and S_2 Δz apart and a curved outer edge. Then the surface integral becomes

$$\iint_S = \iint_{S_1} + \iint_{S_2} + \iint_C$$

If the radius is infinite and Δz infinitely small, then the surface integral over C becomes zero. If we define the quantity to be integrated in the Lorenz equation, $(\mathbf{E}^*\times\mathbf{H}'+\mathbf{E}'\times\mathbf{H}^*)$ to be $F(x,y,z)$, then the Lorenz integral reduces to

$$\iint_S \mathbf{F}\cdot d\mathbf{S} = -\iint_{S_1} F_z(x,y,z)\,dS + \iint_{S_2} F_z(x,y,z)\,dS$$

which equals

$$\iint_S dS\ \{F(x,y,z+\Delta z) - F(x,y,z)\}.$$

Now, letting $dV=\Delta z\,dS$,

$$-j\omega\iiint_V dV(\epsilon-\epsilon')\mathbf{E}^*\cdot\mathbf{E}'$$

becomes

$$-j\omega\Delta z\iint_S(\epsilon'-\epsilon)\mathbf{E}^*\cdot\mathbf{E}'dS$$

and dividing through by Δz, we have

$$\iint_S \frac{d}{dz}F_z(x,y,z) = -j\omega\iint_S(\epsilon'-\epsilon)\mathbf{E}^*\cdot\mathbf{E}'dS$$

Then, decomposing the fields into their transverse (perpendicular to the z axis in Figure 10) and longitudinal (parallel to the z axis) components, i.e. $\mathbf{A} = \mathbf{A}_t+\mathbf{A}_z$, we have with some manipulation,

$$\iint_S \frac{d}{dz}(\mathbf{E}^*\times\mathbf{H}'+\mathbf{E}'\times\mathbf{H}^*)\cdot z \, dS = -j\omega\iint_S(\epsilon'-\epsilon)\mathbf{E}^*\cdot\mathbf{E}'dS \qquad (2.1.5\text{-}4)$$

which is the most useful form of the Lorenz Reciprocity Theorem.

Mode Orthogonality Relations

Before we use the Lorenz reciprocity theorem to develop the relations between coupled waveguide modes, we first observe that the electric and magnetic fields of any mode are orthogonal, that is, if $\mathbf{E}_t$ and $\mathbf{H}_t$ of mode n are defined as

$$\mathbf{E}_t=\mathbf{e}_{n,t}(x,y)\,e^{-j\beta_n z}$$

$$\mathbf{H}_t=\mathbf{h}_{n,t}(x,y)\,e^{-j\beta_n z}$$

then, since they are orthogonal,

$$\iint_S \mathbf{e}_{n,t}\times\mathbf{h}_{m,t}^* = \delta_{n,m}. \qquad (2.1.5\text{-}5)$$

Coupled Modes

As stated above, coupled mode theory works on the assumption that the modes of any perturbed variation on an

original case may be expressed as a linear combination of the modes of the original case. If we assume that the unperturbed case is defined by the electric and magnetic fields

$$\mathbf{E}_t = \sum_n \mathbf{e}_{n,t}(x,y)\, e^{-j\beta_n z}$$

$$\mathbf{H}_t = \sum_n \mathbf{e}_{n,t}(x,y)\, e^{-j\beta_n z}$$

then the perturbed fields $\mathbf{E}_t'$ and $\mathbf{H}_t'$ can be completely defined by

$$\mathbf{E}_t' = \sum_m a_m(z)\, \mathbf{e}_{m,t}(x,y)\, e^{-j\beta_m z}$$

$$\mathbf{H}_t' = \sum_m a_m(z)\, \mathbf{e}_{m,t}(x,y)\, e^{-j\beta_m z}$$

We do not need to include any extra modes or radiation modes. Using $\mathbf{E}_t$, $\mathbf{E}_t'$, $\mathbf{H}_t$, and $\mathbf{H}_t'$ in equation (2.1.5-4), we see the following:

$$\iint_S \frac{d}{dz}\left\{\mathbf{e}_{n,t}^* e^{j\beta_n z} \times \sum_m a_m(z)\, \mathbf{h}_{m,t} e^{-j\beta_m z} + \left(\sum_m a_m(z)\, \mathbf{h}_{m,t} e^{-j\beta_m z}\right) \times \mathbf{h}_{n,t} e^{j\beta_n z}\right\} \cdot \hat{z}\; dS$$

$$= -j\omega \iint_S (\epsilon' - \epsilon) \left(\sum_m a_m(z)\, \mathbf{e}_{m,t}(x,y)\, e^{-j\beta_m z}\right) \cdot \mathbf{e}_{n,t}^*(x,y)\, e^{j\beta_n z}\; dS$$

which can be re-arranged to yield

$$\sum_m \left\{ j(\beta_n-\beta_m)\, a_m(z) + \frac{d}{dz} a_m(z) \right\} e^{j(\beta_n-\beta_m)z} \times \iint_S (\mathbf{e}^*_{n,t} \times \mathbf{h}_{m,t} + \mathbf{e}_{m,t} \times \mathbf{h}^*_{n,t}) \cdot \hat{z}\ dS$$

$$= -j\omega \sum_m a_m(z)\, e^{j(\beta_n-\beta_m)z} \iint (\epsilon' - \epsilon)\ \mathbf{e}_m \cdot \mathbf{e}^*_n\ dS$$

and since

$$\iint_S (\mathbf{e}^*_{n,t} \times \mathbf{h}_{m,t} + \mathbf{e}_{m,t} \times \mathbf{h}^*_{n,t}) \cdot \hat{z}\ dS = 2\delta_{n,m}$$

we have

$$2\frac{d}{dz} a_n(z) = -j\omega \sum_m a_m(z)\, e^{j(\beta_n-\beta_m)z} \iint_S (\epsilon' - \epsilon)\, \mathbf{e}_m \cdot \mathbf{e}^*_n\ dS$$

which leads to the final form used for coupled mode theory,

$$\frac{d}{dz} a_n(z) + j \sum_m a_m(z)\, e^{j(\beta_n-\beta_m)z}\ C_{mn} \qquad (2.1.5\text{-}6)$$

where C_{mn} is the coupling coefficient between modes m and n,

$$C_{mn} = \frac{\omega}{2} \iint_S (\epsilon' - \epsilon)\, \mathbf{e}_m \cdot \mathbf{e}^*_n\ dS \qquad (2.1.5\text{-}7)$$

2.1.5: Coupled Mode Theory

Coupled Waveguides

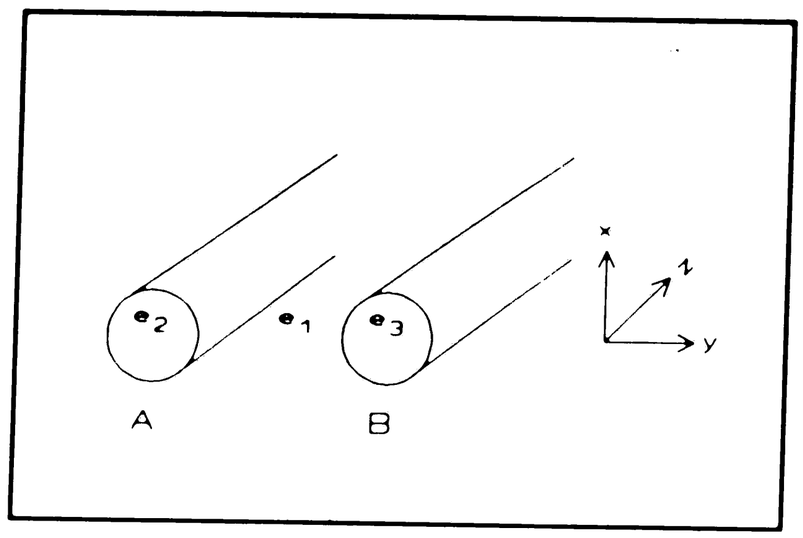

Figure 11

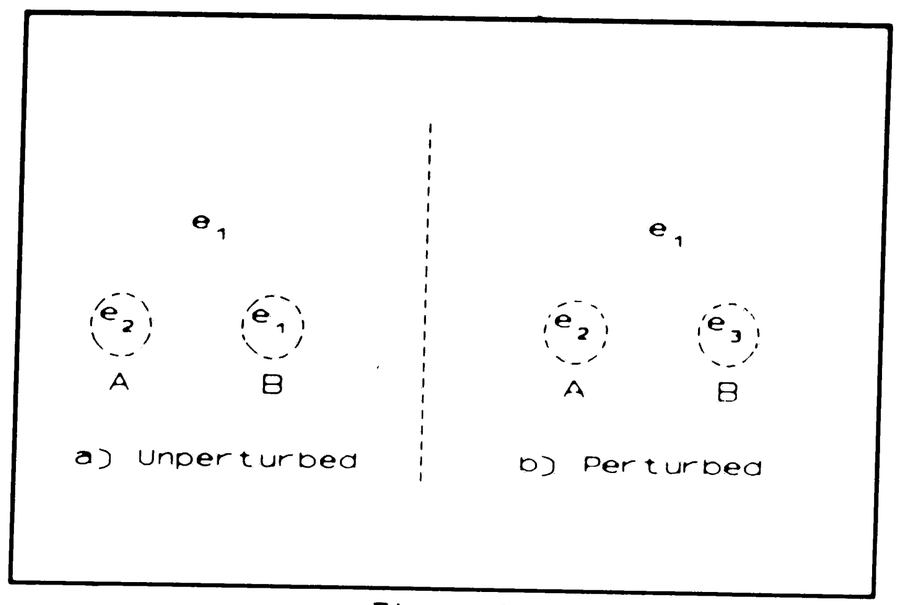

Figure 9

Assume for simplicity waveguides A and B, as shown in figure 11, with permittivity ϵ_1 in the surrounding medium, permittivity ϵ_2 in guide A, and permittivity ϵ_3 in guide B, and that in the unperturbed case (when A and B are isolated), that A and B support only 1 mode. The perturbed and unperturbed cases are depicted in Figure 9. In this case, the perturbation of waveguide A caused by bringing waveguide B into the vicinity is seen in the fact that a region that previously had the dielectric constant ϵ_1 now has the

dielectric constant ϵ_2. If we let

$$\mathbf{E}_A=\mathbf{e}_A(x,y)e^{-j\beta_A z}$$

$$\mathbf{E}_B=\mathbf{e}_B(x,y)e^{-j\beta_B z}$$

be the unperturbed modes, and

$$\mathbf{E}'=a_A(z)\mathbf{e}_A(x,y)e^{-j\beta_A z}+a_B(z)\mathbf{e}_B(x,y)e^{-j\beta_B z}$$

be the perturbed mode, then (2.1.5-6) shows us that

$$\frac{d}{dz}a_A(z)+j\left[a_A(z)C_{AA}+a_B(z)C_{AB}e^{j(\beta_A-\beta_B)z}\right]=0$$

where C_{AA} and C_{AB} are defined by

$$C_{A(A/B)}=\frac{\omega}{2}\iint_{S_2}(\epsilon_2-\epsilon_1)\left[\mathbf{e}_A^*\cdot\mathbf{e}_{(A/B)}\right]dS$$

If we consider the degenerate case where $C_{AB}=0$, then we have

$$\frac{d}{dz}a_A(z)+jC_{AA}a_A(z)=0$$

so

$$a_A(z)=a_{A_0}e^{-jC_{AA}z}$$

so

$$\mathbf{E}_A=a_{A_0}e^{-j(\beta_A+C_{AA})z}$$

We neglect Caa, since

$$\iint_{S_2}\left[\mathbf{e}_A\cdot\mathbf{e}_A^*\right]\cdot dS$$

is negligible in comparison with

$$\iint_{S_2}\left[\mathbf{e}_B\cdot\mathbf{e}_A^*\right]\cdot dS$$

Neglecting C_{AA}, and following the same reasoning for guide B, we have

$$\frac{d}{dz}a_A(z)+ja_B(z)C_{AB}e^{j(\beta_A-\beta_B)z}=0$$

$$\frac{d}{dz}a_B(z)+ja_A(z)C_{AB}e^{-j(\beta_A-\beta_B)z}=0 \qquad (2.1.5\text{-}8)$$

If the waveguides are identical, then $C_{AB}=C_{BA}=\kappa$, and $\beta_A=\beta_B$, so the system of coupled equations becomes

$$\frac{d}{dz}a_A(z)+j\kappa a_B(z)=0$$
$$\frac{d}{dz}a_B(z)+j\kappa a_A(z)=0 \qquad (2.1.5\text{-}9)$$

This system can be solved analytically, and assuming initial excitations of A_0 in guide A and 0 in guide B, the solution is

$$a_A=A_0\cos(\kappa z)$$
$$a_B=\frac{jd}{\kappa dz}a_A=-jA_0\sin(\kappa z)$$

The power P in each guide is proportional to the square of the electric field. $P_A(z)$ and $P_B(z)$ are plotted in Figure 12. The length of complete power transfer is $\kappa L=\frac{\pi}{2}+m\pi$.

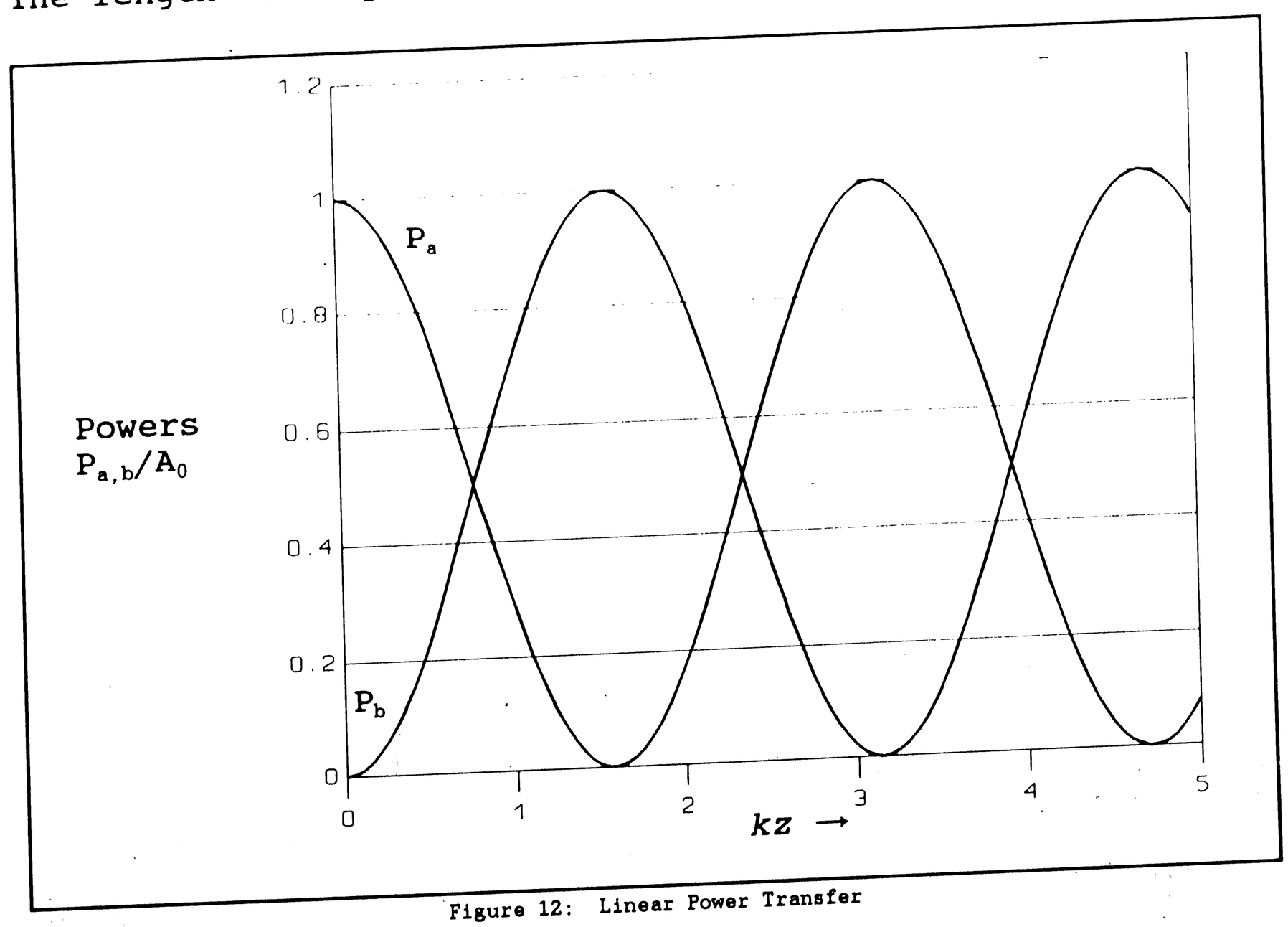

Figure 12: Linear Power Transfer

Detuned Coupler

We now consider the case of the coherent coupler where the propagation constants are not equal, i.e., there exists a detuning δ between β_A and β_B. Such detuning is generally induced by a detuning of the indices of refraction of the waveguides. This is possible using the electro-optic effect, or by fabricating the waveguides out of non-linear materials. We will see that this detuning prevents complete power transfer between the waveguides. First let us note that the coupled mode equations (2.1.5-9) could have been arrived in a slightly different manner. Starting with the same geometry as in Figure 9, assume that the fields $\mathbf{E}_1$ and $\mathbf{E}_2$ are propagating in each waveguide. For each waveguide in the system, assuming only adjacent-waveguide coupling, the following coupled mode equation may be written:

$$j\frac{d}{dz}\mathbf{E}_1+\beta_1\mathbf{E}_1+(\kappa\mathbf{E}_2+\kappa\mathbf{E}_3+\ \ldots\ )$$

For the two-waveguide system, we thus write

$$j\frac{d}{dz}\mathbf{E}_1+\beta_1\mathbf{E}_1+\kappa\mathbf{E}_2=0$$
$$j\frac{d}{dz}\mathbf{E}_2+\beta_2\mathbf{E}_2+\kappa\mathbf{E}_1=0 \qquad (2.1.5\text{-}10)$$

If we use the form $\mathbf{E}_1=a(z)e^{-j\beta_1 z}$, and $\mathbf{E}_2=b(z)e^{-j\beta_2 z}$, and substitute in, we can verify that equations (2.1.5-10) are indeed the same as equations (2.1.5-9). Given certain initial conditions

$a_{(z=0)}=A_0$, $b_{(b=0)}=B_0$, the solution to the detuned case, equation (2.1.5-8), can be expressed as

$$a(z)=e^{-j(\delta/2)z}\left\{A_0\cos\left(\frac{\kappa}{F}z+j\left(B_0+\frac{\delta}{2\kappa}A_0\right)\sin\left(\frac{\kappa}{F}z\right)\right)\right\}$$

$$b(z)=e^{+j(\delta/2)z}\left\{B_0\cos\left(\frac{\kappa}{F}z+j\left(A_0+\frac{\delta}{2\kappa}B_0\right)\sin\left(\frac{\kappa}{F}z\right)\right)\right\}$$

where $\delta=\beta_1-\beta_2$ and $F=(1+\frac{\delta^2}{4\kappa^2})^{-\frac{1}{2}}$. We may verify that if $a_{10}=A_0$, $b_{10}=B_0$, $\delta=0$, and $F=1$, we have the non-detuned case. If $a_{10}mA_0$, $b_{10}=0$, and $\delta\neq0$, we can solve for the powers in the waveguides

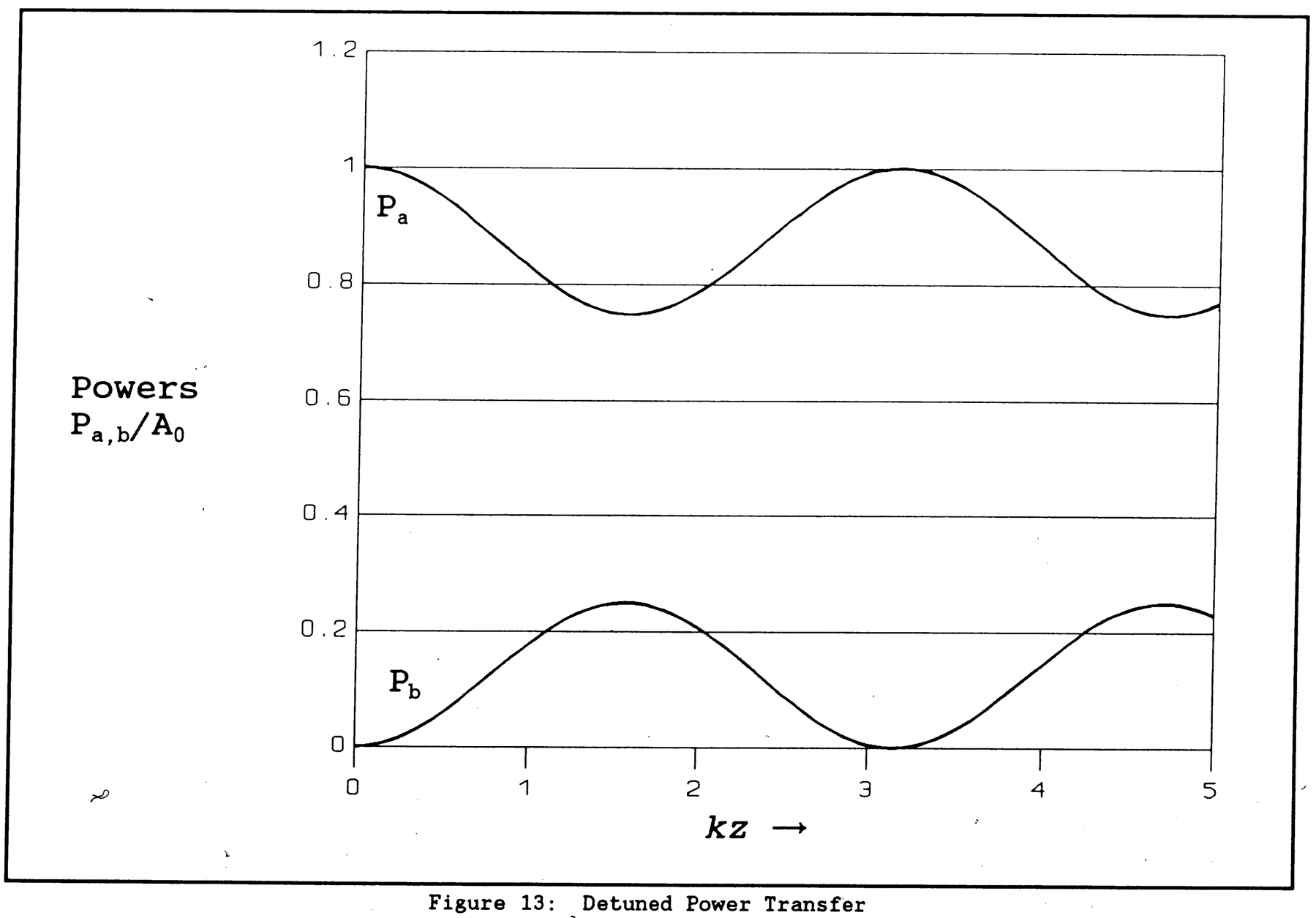

Figure 13: Detuned Power Transfer

as a function of z, yielding

$$P_a=|A_0|^2\left[1-F^2\sin^2\left(\kappa\frac{z}{F}\right)\right]$$

$$P_b=|A_0|^2F^2\sin^2\left(\kappa\frac{z}{F}\right)$$

P_a and P_b for a detuned coupler are plotted in Figure 13. The length at which maximum power transfer occurs is still $L=\pi/2k$.

Supermodes

For the coherent coupler discussed above, there exist certain power distributions at which no power transfer occurs. These are designated "normal modes", or supermodes, and are stable modes of the coupled configuration*1. If we rewrite equation (2.1.5-10) in matrix form, we can see that

$$j\frac{d}{dz}\begin{bmatrix}\mathbf{E}_1\\ \mathbf{E}_2\end{bmatrix}+\begin{bmatrix}\beta & \kappa\\ \kappa & \beta\end{bmatrix}\begin{bmatrix}\mathbf{E}_1\\ \mathbf{E}_2\end{bmatrix}=0$$

or

$$j\bar{E}'+\bar{M}\ \bar{E}=0$$

Following standard differential equation solving techniques, we assume $\bar{E}=\bar{E}_0e^{j\sigma z}$, and we are led to the eigenvalue equation (for sigma) $(\sigma-\beta)^2=\kappa^2$, with solutions $\sigma_1=\beta+k$ and $\sigma_2=\beta-k$. These solutions lead quickly to the two eigenvectors $\begin{bmatrix}1\\1\end{bmatrix}$ and $\begin{bmatrix}1\\-1\end{bmatrix}$. These eigenvectors represent the two supermodes of the two-waveguide coupler. If power is injected into the coupler in either of these two combinations, no coupling will occur. If

*1 Note that the usage of the term mode is more general here, meaning state of the entire coupled system.

we normalize the two supermodes and let

$$|1\rangle = \frac{1}{\sqrt{2}}\begin{bmatrix}1\\1\end{bmatrix},\quad |2\rangle = \frac{1}{\sqrt{2}}\begin{bmatrix}1\\-1\end{bmatrix}$$

then the state $|\Psi\rangle$ of the waveguide may be represented as a linear combination of these supermodes,

$$|\Psi\rangle = C_1|1\rangle e^{j\sigma_1 z} + C_2|2\rangle e^{j\sigma_2 z}$$

where C_1 and C_2 come from the initial conditions. If we know Ψ_0, then $C_1=\langle 1|\Psi_0\rangle$ and $C_2=\langle 2|\Psi_0\rangle$. If Ψ_0 is $\begin{bmatrix}A_0\\B_0\end{bmatrix}$, then $C_1=\frac{1}{\sqrt{2}}(A_0+B_0)$ and $C_2=\frac{1}{\sqrt{2}}(A_0-B_0)$, and

$$|\Psi\rangle = \frac{A_0+B_0}{\sqrt{2}}\cdot\begin{bmatrix}1\\1\end{bmatrix}\frac{1}{\sqrt{2}}e^{j(\beta+\kappa)z} + \frac{A_0-B_0}{\sqrt{2}}\cdot\begin{bmatrix}1\\-1\end{bmatrix}\frac{1}{\sqrt{2}}e^{j(\beta-\kappa)z}$$

Section 2.1.6: Two-Waveguide Nonlinear Coherent Coupler

The above discussion has been conducted for a two-core linear coupler, i.e., with no allowance for non-linearities. We next consider the case of a simple two-waveguide directional coupler fabricated out of non-linear materials, i.e., materials whose index of refraction varies with the amount of power propagating. The power flowing in each waveguide will affect its index of refraction, and thus affect the propagation constant β_n in that waveguide. This will result in a detuning of the two waveguides which is dependent upon the amount of power flowing, which will result in power-dependent coupling. The Nonlinear Coherent Coupler (NLCC) was first described in 1980 by Jensen, [5]. For the two-waveguide

nonlinear coherent coupler, it is possible to derive an analytical solution for the coupling as a function of z.

Self-Phase Modulation

The next factor to be introduced in our discussion is the effect that non-linearities have on the coupled mode equations. As discussed above, for non-linear materials, $n=n_0+n_2|\mathbf{E}|^2$. If we take the Helmholz vector equation, (2.1.1-9), note that $\nabla^2 = \frac{\delta^2}{\delta z^2}$, and use $\mathbf{E}=E(z)e^{j\beta_0 z}e^{j\omega t}$, and note that since $n_2|\mathbf{E}|\ll n_0$, $n^2=n_0^2+2n_0n_2|\mathbf{E}|^2$, we have

$$e^{j\beta_0 z}\left[\ddot{E}(z)+2j\beta_0\dot{E}(z)-\beta_0^2E(z)\right]+\frac{(n_0^2+2n_0n_2|E(z)|^2)\omega^2}{c^2}E(z) = 0$$

Now, the $\ddot{E}(z)$ term can be neglected due to the standard slowly varying envelope approximation, and the $-\beta_0^2E(z)e^{j\beta_0 z}$ term cancels with the n_0^2, and with some manipulation we are left with

$$j\dot{E}(z)+\frac{n_2\omega}{c}|E(z)|^2E(z)=0. \qquad (2.1.6\text{-}1)$$

The $|E(z)|^2$ term is known as a self-phase modulation term, and is a direct result of the dependence of the index of refraction on the power flowing. A direct modification to equations (2.1.5-10) may then be made, yielding

$$j\dot{E}_1(z) + \beta E_1(z) + \kappa E_2(z) + \frac{n_2\omega}{c}|E_1(z)|^2E_1(z)=0$$

$$j\dot{E}_2(z) + \beta E_2(z) + \kappa E_1(z) + \frac{n_2\omega}{c}|E_2(z)|^2E_2(z)=0 \qquad (2.1.6\text{-}2)$$

which are the two-core non-linear coupled mode equations. These are similar in form to those of [6]. The coupling coefficients κ are determined by the geometries of the waveguides.

Normalization

At this point it is helpful to convert to a normalized system of equations, similar to those of section (above). We will use this normalized system of equations for the remainder of this thesis, occasionally converting back when actual numerical examples are presented. Equations (2.1.6-2) may be re-written, as in §2.1.5, letting $E_1(z)=a(z)e^{-j\beta z}$ and $E_2(z)=b(z)e^{-j\beta z}$, and $\lambda=\frac{n_2\omega}{c}$ to yield

$$j\frac{d}{dz}a(z) + \kappa b(z) + \lambda|a(z)|^2a(z)=0$$
$$j\frac{d}{dz}b(z) + \kappa a(z) + \lambda|b(z)|^2b(z)=0.$$

If we make a transformation of variables, letting the dimensionless $\eta=\mu z$, then $\frac{d}{dz}=\mu\frac{d}{d\eta}$, then we have

$$j\frac{d}{d\eta}a(z) + \frac{\kappa}{\mu}b(z) + \frac{\lambda}{\mu}|a(z)|^2a(z)=0$$
$$j\frac{d}{d\eta}b(z) + \frac{\kappa}{\mu}a(z) + \frac{\lambda}{\mu}|b(z)|^2b(z)=0.$$

Then if we make a further transformation of variables, letting $A=a\left[\frac{\lambda}{\mu}\right]^{\frac{1}{2}}$ and $B=b\left[\frac{\lambda}{\mu}\right]^{\frac{1}{2}}$, then equations (E) become

$$j\frac{d}{d\eta}A + \left[\frac{\kappa}{\mu}\right]B + |A|^2A = 0$$
$$j\frac{d}{d\eta}B + \left[\frac{\kappa}{\mu}\right]A + |B|^2B = 0 \qquad (2.1.6\text{-}3)$$

Equations (2.1.6-3) may be solved analytically, using the following combinations of A and B analogous to the Stokes parameters:

$$S_0=|A|^2 + |B|^2$$

$$S_1=|A|^2 - |B|^2$$

$$S_2=AB^* + A^*B$$

$$S_3=j(A^*B - AB^*).$$

Letting $K=\left[\frac{\kappa}{\mu}\right]$, the evolution equations for these parameters are found to be

$$\frac{d}{d\eta}S_0=0$$

$$\frac{d}{d\eta}S_1=2KS_3$$

$$\frac{d}{d\eta}S_2=-KS_1S_3$$

$$\frac{d}{d\eta}S_3=-2KS_1+S_1S_2.$$

Two constants are observable in this system, determined by initial conditions $S_1(0)$, $S_2(0)$, $S_3(0)$,

$$S_0^2=S_1^2+S_2^2+S_3^2=R^2, \text{ and}$$

$$\Gamma=S_2+\frac{S_1^2}{4K}$$

which allow for a complete description of the motion of the parameters. With some manipulation we may arrive at the equation for S_1

$$\ddot{S}_1+\alpha S_1+\beta S_1^3=0, \qquad (2.1.6\text{-}4)$$

where

$$\alpha=4K^2-2K\Gamma,$$

$$\beta=\frac{1}{2}.$$

Equation (2.1.6-4) is analytically solvable in terms of elliptic functions. Let us assume that power is initially injected into only one waveguide, so that $a(0)=A+j0$, and $|a(0)|=A$, and $|a(0)|^2=A^2$. The solutions will fall into two classes, depending upon whether or not the initial power A is greater or less than some critical power A_c. This translates into a condition on R and Γ, with the critical condition being $R=\Gamma$. When $R=\Gamma$, simple substitution leads to $A=2\sqrt{K}$. When $R>\Gamma$, which corresponds to $A<2\sqrt{K}$, the following solution lends itself:

$$S_1=A^2\mathrm{cn}\left[\eta(a+bA^4)^{\frac{1}{2}},\lambda\right],\quad \lambda^2=\frac{bA^4}{2(a+bA^4)}$$

where cn[] is the incomplete Jacobian function with modulus λ. $|a(\eta)|^2$ and $|b(\eta)|^2$ can be easily solved for,

$$|a(\eta)|^2=\frac{S_0+S_1}{2},$$

$$|b(\eta)|^2=\frac{S_0-S_1}{2}.$$

Therefore, whenever the input power A into waveguide a is less than $2\sqrt{K}$, the expressions for $|a(\eta)|^2$ and $|b(\eta)|^2$ are:

$$|a(\eta)|^2=\frac{S_0+S_1}{2}=\frac{A^2}{2}+\frac{A^2}{2}\mathrm{cn}\left[\eta(a+bA^4)^{\frac{1}{2}},\lambda\right]$$

$$|b(\eta)|^2=\frac{S_0-S_1}{2}=\frac{A^2}{2}-\frac{A^2}{2}\mathrm{cn}\left[\eta(a+bA^4)^{\frac{1}{2}},\lambda\right]$$

with λ defined above. For a simple case, consider $K=1$ in equations (2.1.6-3). We then have

$$|a(\eta)|^2=\frac{A^2}{2}+\frac{A^2}{2}\mathrm{cn}\left[2\eta,\frac{A^2}{4}\right],$$

$$|b(\eta)|^2=\frac{A^2}{2}-\frac{A^2}{2}\mathrm{cn}\left[2\eta,\frac{A^2}{4}\right],$$

$$\lambda=\frac{A^2}{4}.$$

These results are plotted in Figure 14 for A=1.9. The function is periodic with period $4K(\lambda)$, where $K(\lambda)$ is the complete jacobian elliptic function with modulus λ. After a distance $K(\lambda)$, 50% power transfer has taken place, after $2K(\lambda)$, 100% power transfer, after $3K(\lambda)$, the powers have reversed back to 50%, and after $4K(\lambda)$, the original power distributions are present. It should be noted that when λ is small, that is when A≪2, the system approaches behaving like the linear coupled-mode equations described in §2.1.5, i.e. sinusoidal transfer of the powers. When R<Γ, a similar

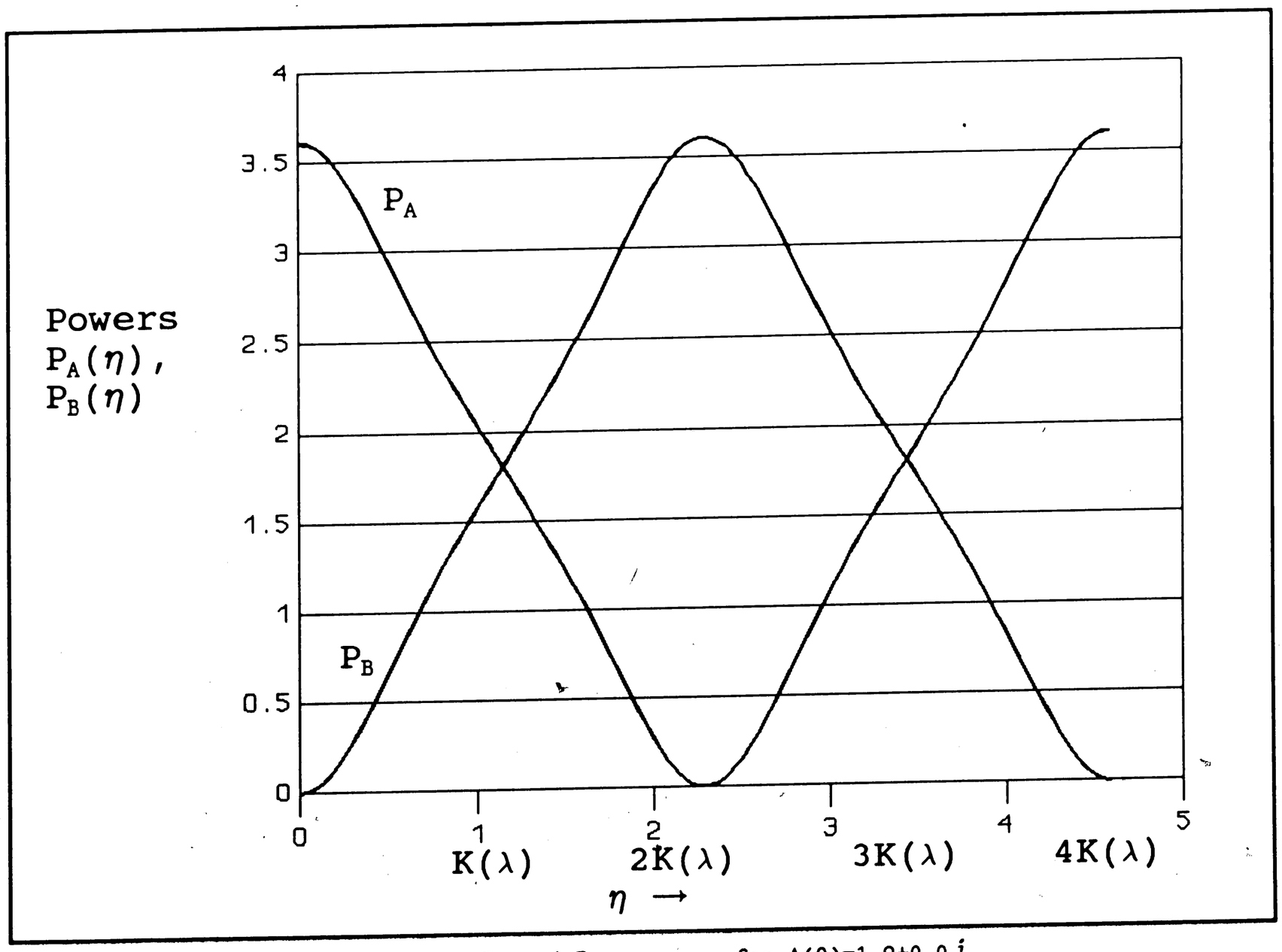

Figure 14: P_A and P_B versus η for A(0)=1.9+0.0j

analysis can be performed, leading to the general solution

$$|a(\eta)|^2 = \frac{S_0+S_1}{2} = \frac{A^2}{2} + \frac{A^2}{2}\mathrm{dn}\left[\eta A^2\left(\frac{b}{2}\right)^{\frac{1}{2}}, \lambda\right],$$

$$|b(\eta)|^2 = \frac{S_0-S_1}{2} = \frac{A^2}{2} - \frac{A^2}{2}\mathrm{dn}\left[\eta A^2\left(\frac{b}{2}\right)^{\frac{1}{2}}, \lambda\right],$$

$$\lambda^2 = 2\left[1-\frac{a}{bA^4}\right].$$

As a specific case, consider A=2.1 and K=1. The results are plotted in Figure 15. Note that the solution is periodic with period $2K(\lambda)$, and that complete power transfer never occurs. This case is similar to the detuned coupler discussed in §2.1.5.

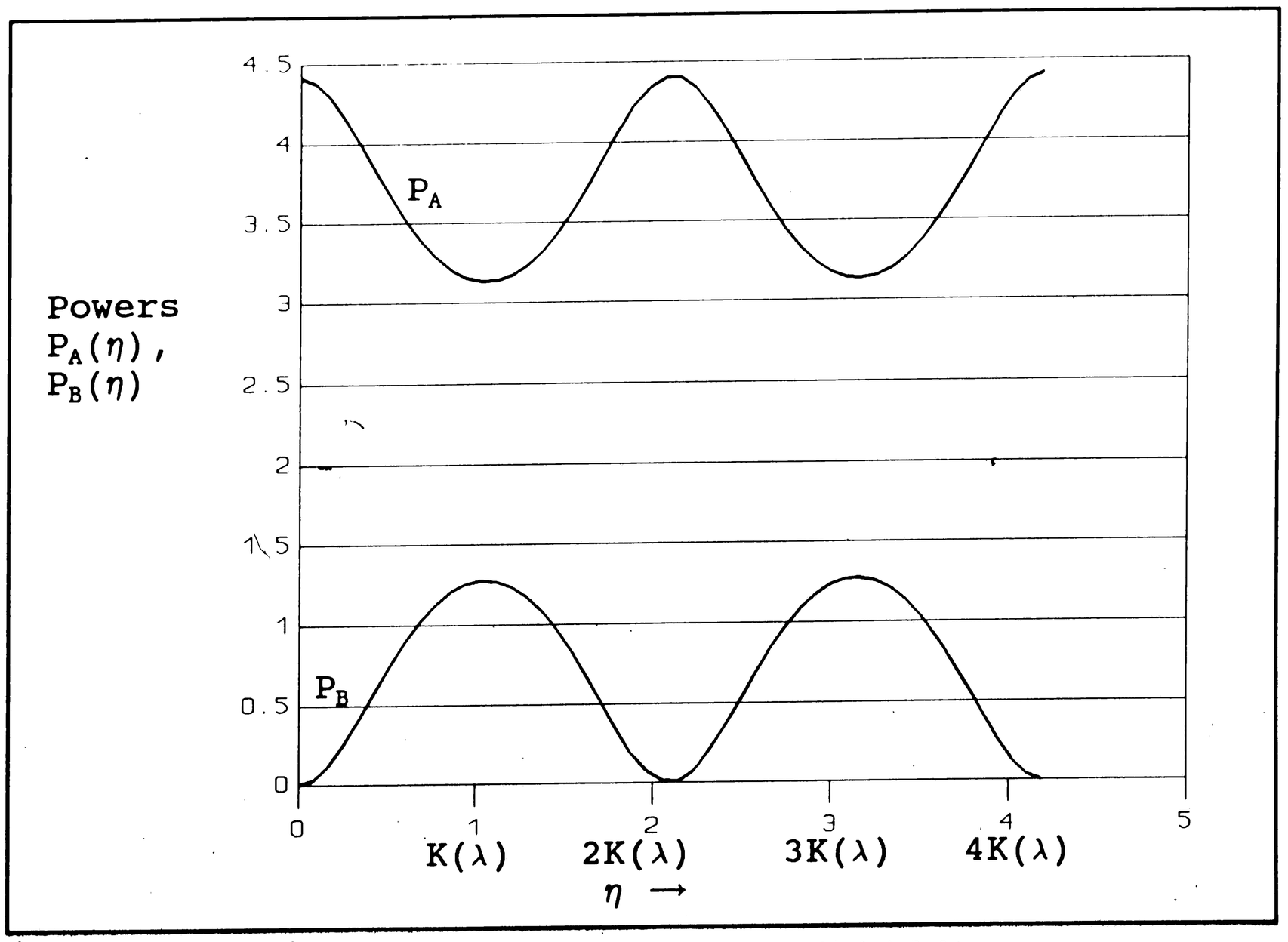

Figure 15: P_A and P_B versus η for A(0)=2.1+0.0j

Computer Simulation

As an exercise, before the computer simulation of the bi-directional NLCC of §3.3, a computer program was written to simulate the two-core NLCC examined above. To allow simulation, the system of 2 equations in 2 unknowns described above (equations (2.1.6-3)), was re-written into 4 equations in 4 unknowns by decomposing each equation into its real and imaginary components, i.e. letting $a=a_r+ja_i$ and $b=b_r+jb_i$, and plugging in, and separating the real and imaginary components of each equation. The resulting set of equations is

$$\dot{a}_i=Kb_r+a_r^3+a_ra_i^2$$

$$\dot{a}_r=-(Kb_i+a_i^3+a_ia_r^2)$$

$$\dot{b}_i=Ka_r+b_r^3+b_rb_i^2$$

$$\dot{b}_r=-(Ka_i+b_i^3+b_ib_r^2)$$

with initial conditions $a_i(0)$, $a_r(0)$, $b_i(0)$, and $b_r(0)$ and coupling coefficient K to be specified. Then, the fourth order Runge-Kutta method was applied. The flowchart for this program is in Figure 16. Given any initial conditions, step size, and coupling coefficient, it solves the system step by step, from $\eta=0$, h, $2h$, $3h$, etc. Figures 14, 15, 17, and 18 were generated from the output of this program.

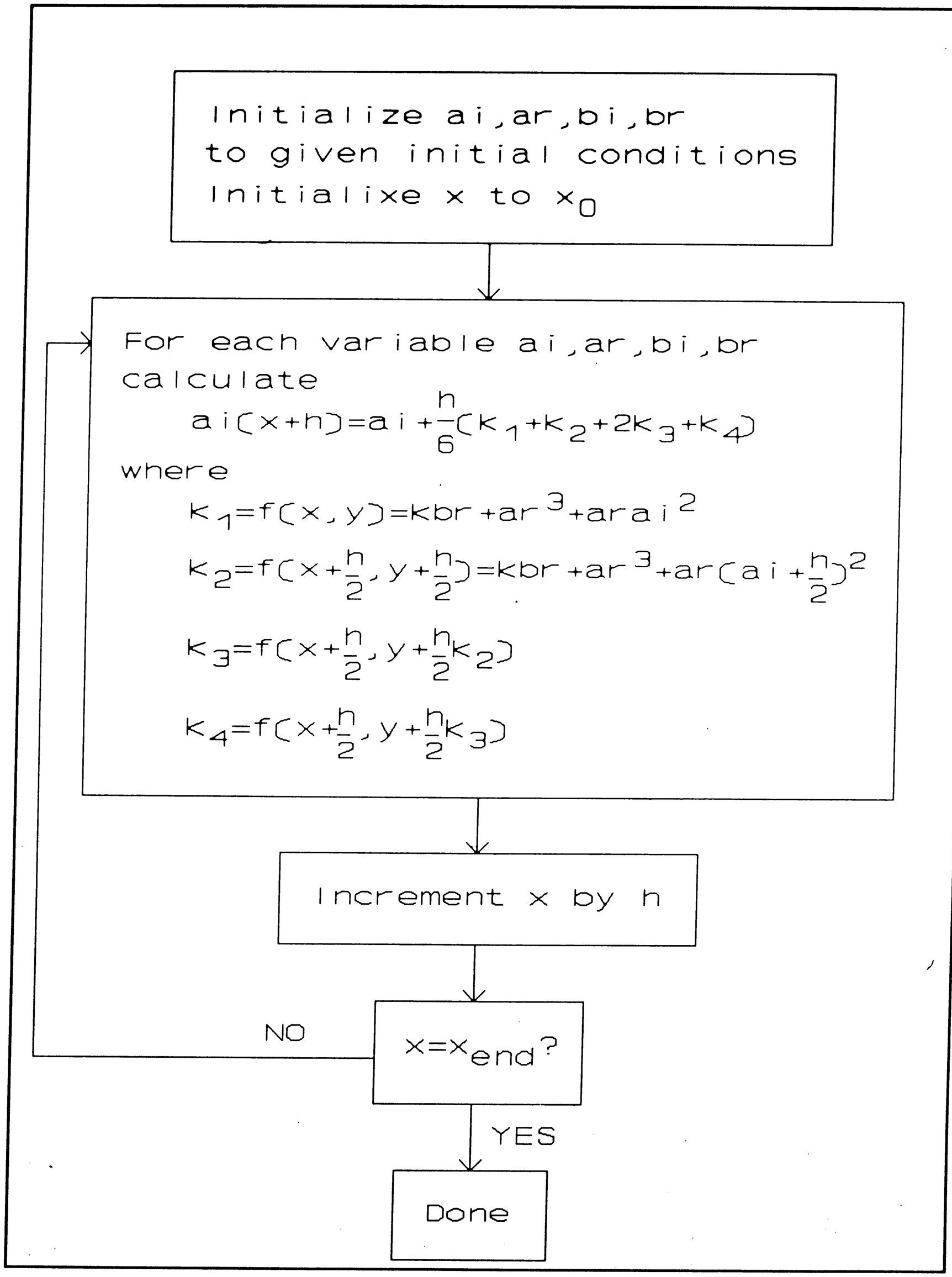

Figure 16: Flowchart for Unidirectional NLCC

2.1.6: NLCC

Applications of the Nonlinear Coherent Coupler

Since it was introduced in 1980, the Nonlinear Coherent Coupler (NLCC) has received considerable attention in the literature. Because of the strange behavior of this device, it is feasible to use it as an optical logic gate, as a pulse-narrowing device, and other applications. Jensen [4] first proposed using the NLCC as an optical logic gate, specifically calculating the length and powers required to create an optical 'NOT' gate. Consider a NLCC operating with an input power P_{in} in guide A less than P_c, so that the 100% power transfer condition is reached at a certain η, at which point the output of guide B is $P_{out}=P_{in}$, and the output of guide A is zero (see Figure 17). When P_{in} is increased, less of the power

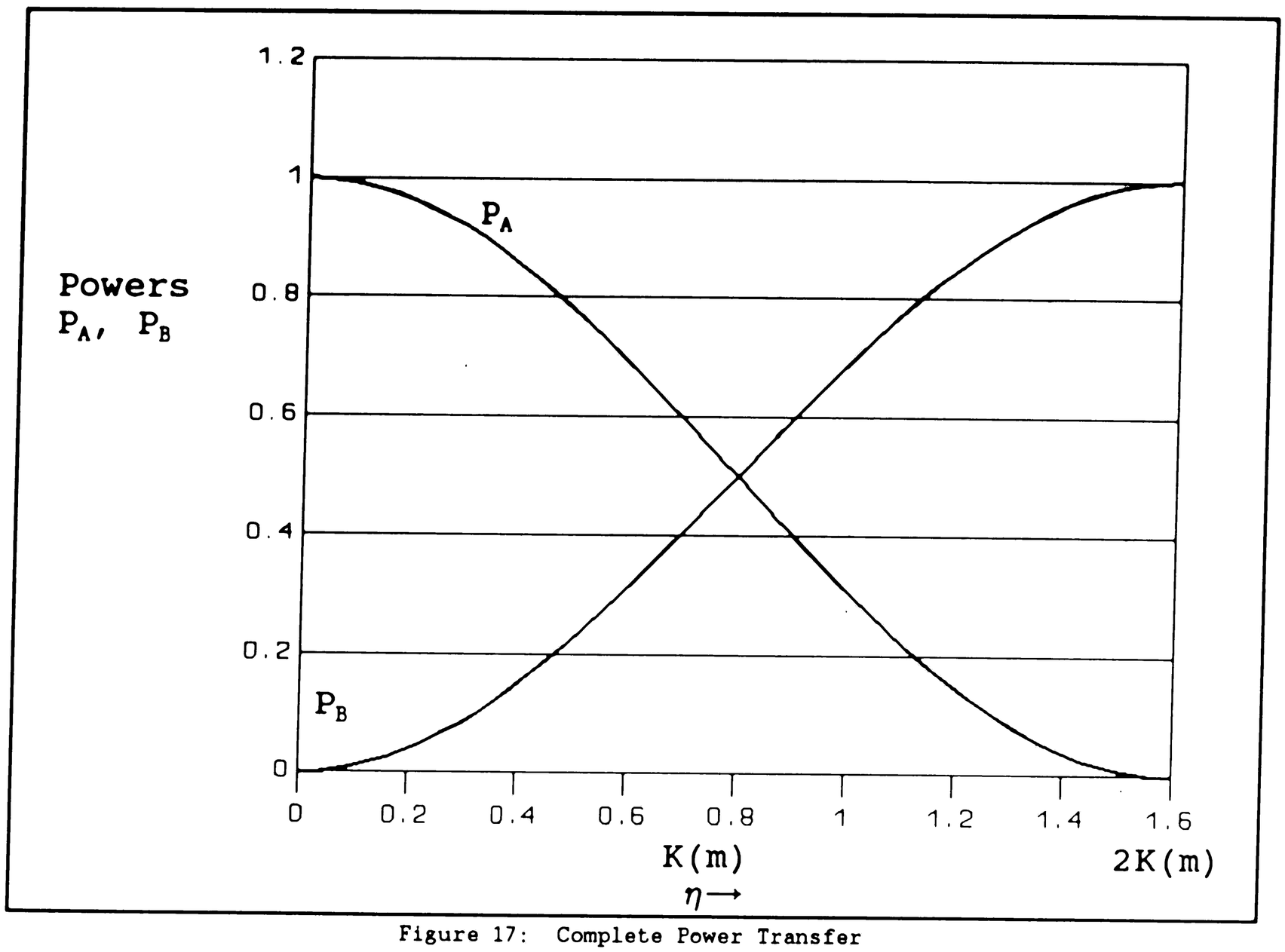

Figure 17: Complete Power Transfer

couples into guide B, and more of the power remains in guide A, causing the device to switch from the crossed state to a parallel state, where half of the power remains in guide A (see Figure 18). For a complete switch to take place at a give length L, the period of transfer $2K(m)$ must change. If $L=2K(m)$ (the device is exactly long enough to allow one 100% power transfer to be reached), and we wish an increase in P_{in} to result in a switch from the output appearing in guide B to half of the output appearing in each guide, then the input power must change sufficiently to cause $L=K(m)$ in the switched state. In our normalized system, if we arbitrarily choose an

input power for the crossed state of A(0)=1.0+0.0j, then this equates to a coupler of normalized length $2K(1.0^2/4.0^2) = \eta$ =1.5963. Then if we increase the input power to A'(0) so that at length 1.5963 the power is equally split between the 2 guides, we see that the necessary change in $K(m)$ is $K(m') = 2K(m)$. Thus $K(m')$ = 3.195, requiring A'(0) to be 1.986. Jensen calculated that if there are two waveguides with K=3.14 cm^{-1}, 0.5 cm exchange length, cross sectional area A=3μm^2, λ=1.06 μm, n_0=3.5, $n_2=5^{-10}$ ESU, then the critical input power is 10.6 Watts. Although this power seems quite high, we must

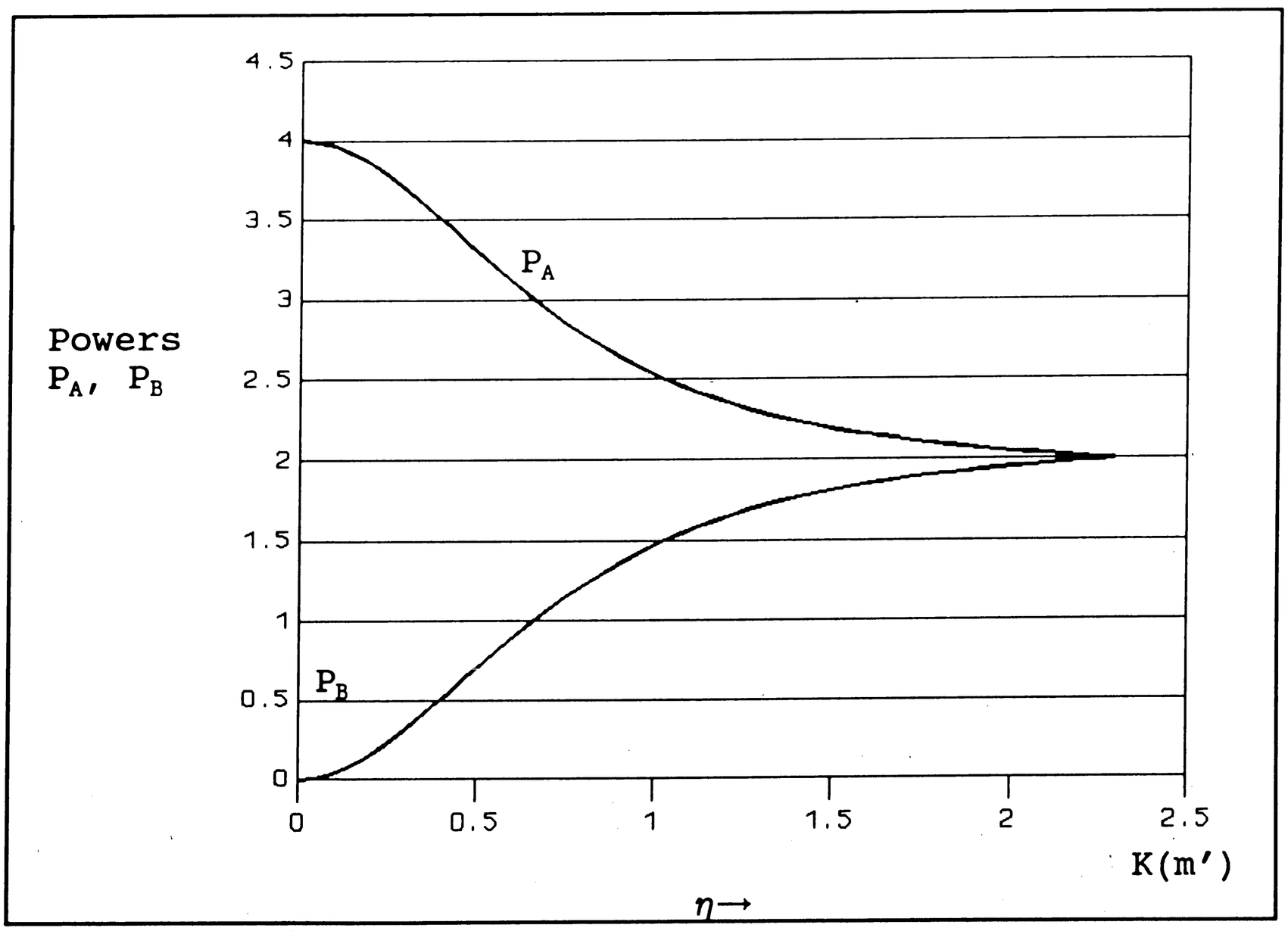

Figure 18: 50% Power Transfer

keep in mind that the device is capable of exceedingly fast switching times, which are not limited by propagation time (since the fields interact in a spatially and temporally local fashion), but only by the nonlinear response time of the material, which, as discussed above, can be on the order of femtoseconds. Other papers[7, 8, 9, 10, 11] have explored the ultrafast all-optical switching capabilities of the NLCC. There have also been studies[12] directed at using the NLCC for optical pulse compression. Using the same geometry as discussed above, and injecting a bell-shaped pulse to be narrowed into guide A, we observe that in the (temporal) beginning of the pulse, when the input is yet relatively 'low', the NLCC will act to couple that power away from guide A and into guide B. As the input power increases, later in the pulse, and reaches a maximum, the NLCC will cease to couple the power from guide A to guide B, and the power will remain in guide A. At the end of the pulse, when the input into guide A is low again, the NLCC will couple this power from guide A to guide B. The shape of the pulse that emerges at the output of guide A is a much sharper pulse. This is illustrated in Figure 19. Kitayama and Wang [12] have predicted that pulse compression to less than 1/5 is attainable with loss of approximately 3 dB.

The NLCC as an Optical Amplifier

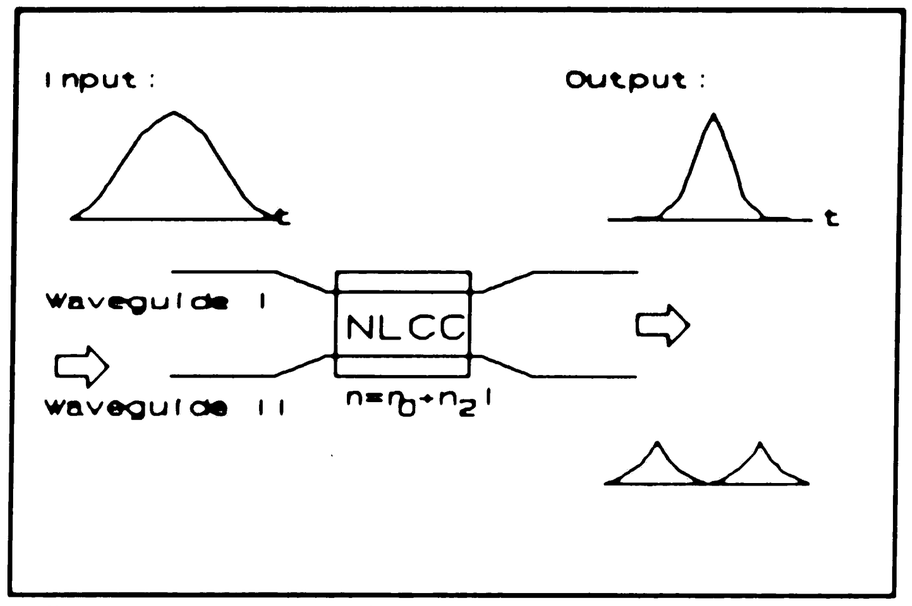

Figure 19: Optical Pulse Compression via NLCC

A(0)=1.9+j0.0, L=4.5830

B(0)	Gain	B(0)	Gain
.01∠0°	55.2	.02∠0°	562.5
.01∠30°	38.9	.02∠30°	399.2
.01∠45°	24.6	.02∠45°	250.8
.01∠60°	11.2	.02∠60°	112.6
.01∠90°	1.4	.02∠90°	1.8
.01∠120°	14.7	.02∠120°	142.0
.01∠135°	26.7	.02∠135°	249.1
.01∠150°	37.8	.02∠150°	344.1
.01∠180°	47.1	.02∠180°	419.2

Figure 20: Gain as a Function of Phase

In the configuration we are currently considering, the only possible way to use the NLCC as an amplifier is to have the NLCC operating at a certain steady state, with a constant power A_0 flowing into, say, guide A (see Figure 17), and zero power B_0 entering guide B. Then we may choose the proper length $4K(\lambda)$ at which the output from guide B is nominally zero. Any perturbations on the input conditions, either on the power entering guide A or the power entering guide B will cause perturbations on the outputs of guides A and B. It is possible to operate the device with the power entering guide A, A_0, very close to the "saddle" point discussed above (A_c=2.0 in our normalized system). Then any small variations in either A_0 or B_0 will cause large variations in the outputs A_L and B_L. The major problem with operation as such is that the system is not only sensitive to the amplitude of the perturbations, but also the phase. As shown in Figure 14,

when A_0=1.9+j0, and B_0=0+j0, the output from guide B at length η=4.5830 is zero. When a small perturbation is introduced at B_0, say ΔB_0=0.01+j0.0, then the output B_L changes to .05513, a power gain of 551.3. When another small perturbation of the same magnitude but different phase is introduced at B_0, the output B_L changes to .00013, a power gain of 1.3. Further examples are listed in Figure 20. As the reader can see, the output of the amplifier used in this configuration is a function not only of the amplitude of the input signal, but of the phase of the input signal. The operation of the amplifier is therefore far from ideal. An amplifier whose amplification depends solely upon the magnitude of the input signal is described in the next section.

Section 2.2: Numerical Techniques

The behaviors of the optical devices studied in this thesis are described by systems of ordinary differential equations. When the systems become complicated, closed-form solutions become impossible to calculate. The techniques discussed in this section, however, can solve most of the systems of differential equations numerically to practically any degree of accuracy.

2.2: Numerical Techniques

Consider the solution of the *n*th order ordinary differential equation of the form

$$F\left\{x, y, \frac{dy}{dx}, \frac{d^2y}{dx^2}, \frac{d^3y}{dx^3}, \ldots, \frac{d^ny}{dx^n}\right\} = 0. \qquad (2.2\text{-}1)$$

An equation of this type is termed *n*th order because the highest derivative is of order *n*, and ordinary because only total derivatives appear (no partial derivatives present, or alternatively, there is only one independent variable, *x*). To obtain a unique solution to (2.2-1), it is necessary to supply some additional information, namely, values of $y(x)$ and/or of its derivatives at some specific values of *x*. For an *n*th order equation, *n* such conditions must be provided to determine a unique solution $y(x)$. If all *n* of the conditions are provided at some particular *x*, then the problem is termed an initial value problem. When more than one value of *x* is involved, the problem is termed a boundary-value problem. An *n*th order differential equation may always be re-written into *n* first-order differential equations by introduction of *n-1* additional variables. The solutions of systems of first-order ordinary differential equations are merely expansions upon the single-variable methods.

Initial Value Problems

2.2: Numerical Techniques

One method of solution of first order ordinary differential equations,

$$\frac{dy}{dx} = f(x,y) \qquad (2.2\text{-}2)$$

is known as Taylor's method. This method involves expressing the solution $y(x)$ about some starting point x_0 by using a Taylor's expansion ([13], ch.6):

$$y(x_0 + h) = y(x_0) + hf(x_0,y(x_0)) + \frac{h^2}{2!}f'(x_0,y(x_0)) + \frac{h^3}{3!}f''(x_0,y(x_0)) + \ldots \qquad (2.2\text{-}3)$$

If $y(x_0)$ is specified as the initial condition, $f(x_0,y(x_0))$ can be computed directly from equation (2.2-2). To evaluate the higher-order derivatives in (2.2-3), we differentiate $f(x,y)$ using the chain rule, since f is a function of both x and y:

$$\frac{df}{dx} = \frac{\delta f}{\delta x} + \frac{\delta f}{\delta y}\frac{dy}{dx} \qquad (2.2\text{-}4)$$

Unfortunately, in the general case, differentiation of $f(x,y)$ becomes prohibitively complicated. Except for a first order estimate, with error of order $O(h^2)$, Taylor's expansion is not often used to solve first-order differential equations.

It is possible, however, to develop one-step procedures which involve only first-order derivative evaluations but which produce results equivalent in accuracy to the higher-order Taylor methods. These algorithms are known as the Runge-Kutta methods. The most common of these methods, and possible the most widely used single step method for solving

ordinary differential equations, is the fourth order Runge-Kutta method with Gill constants ([13]). The fourth-order formula is of the form

$$y_{i+1} = y_i + \frac{h}{6}(k_1 + 2k_2 + 2k_3 + k_4) \qquad (2.2\text{-}5)$$

where

$$k_1 = f(x_i,\ y_i),$$

$$k_2 = f(x_i + \tfrac{1}{2}h, y_i + \tfrac{1}{2}hk_1),$$

$$k_3 = f(x_i + \tfrac{1}{2}h, y_i + \tfrac{1}{2}kh_2),$$

$$k_4 = f(x_i + h, y_i + hk_3).$$

The step error involved in the m-th order Runge Kutta method is $O(h^{m+1})$. Therefore, when solving a system using step size $h=1x10^{-2}$ with the fourth order Runge-Kutta method, the error in each step is $O(1x10^{-10})$. This method can provide very accurate results.

Boundary Value Problems

In problems in which the initial conditions are given at more than one value of the independent variable, the solutions are considerably more complicated. Two families of algorithms are common for solving boundary-value problems; finite difference methods and shooting methods.

Finite difference methods involve approximation of the differential equation at $n + 2$ points x_0, x_1, ..., x_{n+1}. Each derivative is replaced by a finite-difference representation.

Then, for two-point boundary value problems, the initial conditions $y(x_0=a)=y_0=\alpha$ and $y(x_{n+1}=b) =y_{n+1}=\beta$ are placed directly into the 0^{th} and $(n+1)^{st}$ equation, and the procedure leads to a system of n simultaneous equations in the unknowns y_1, y_2, ..., y_n. Obviously, if many intermediate data points are desired, this method may not be practical. If the original equation is linear (no higher variable or derivative of a variable appears to the second or higher power), then the resulting set of equations is linear, and may be solved using Gaussian elimination methods. If the original equation is non-linear, the system of finite-differential equations generated is also nonlinear. The generation of any solution of such a system may be very difficult. In some cases, one may linearize the equations, solve the equations, re-linearize about the new solution, and so on, until full non-linearity is reached and a solution is found. In effect, a complicated problem is replaced by many less complicated problems. However, this approach does not guarantee a solution.

The shooting methods reduce the solution of the boundary-value problem into the iterative solution of an initial-value problem. The boundary at which the most initial conditions are known is chosen as a starting point, and an initial-value method such as the Runge-Kutta method discussed above is used to solve iteratively, toward the other boundary. The computed solution at the second boundary is compared with the known

solution, and adjustments are made. This trial-and-error approach may be successful when applied to linear or nearly-linear equations, but for fully non-linear equations may prove as unsatisfactory as the finite-difference methods.

As should be apparent from the preceding paragraphs, there are no known algorithms which guarantee the solution of a boundary-value ordinary differential equation, particularly a highly non-linear one.

Section 2.3: Elliptic Functions

A class of functions exists in the annals of mathematics which may be used to solve some equations which would not normally be analytically solvable using standard sinusoidal functions. This class of functions is known as the Jacobian Elliptic Functions. The theory of elliptic functions, first developed in 1826 by Abel and Jacobi ([14]), can be used to develop a closed form solution to, in particular, the unidirectional evolution of the fields in a Nonlinear Coherent Coupler. The use of the elliptic functions to solve the equation

$$\ddot{y} + ay + by^3 = 0, \qquad (2.3\text{-}1)$$

where $a>0$, $b\neq 0$, and $y(0)=y_0$, $\dot{y}(0)=0$, is presented here, adapted from ([15]).

2.3: Elliptic Functions

Before the solution is presented, however, the definition of the Elliptic integrals of the first kind is presented. Elliptic integrals of the first kind are represented by ([41])

$$F(k,\phi) = \int_0^{\phi} \frac{d\phi}{\sqrt{1 - k^2\sin^2\phi}}$$

$$= \int_0^{x} \frac{d\xi}{\sqrt{(1-\xi^2)(1-k^2\xi^2)}}, \quad x=\sin\phi, \quad k^2<1. \tag{2.3-2}$$

k is called the modulus, and ϕ is called the amplitude of the elliptic function. if $u=F(k,\phi)$, then the following quantities are defined:

$k' = (1 - k^2)^{\frac{1}{2}}$ is the complementary modulus, (2.3-3)

$\sin\phi = \text{sn}u = x$, (2.3-4)

$\cos\phi = \text{cn}u = (1-x^2)^{\frac{1}{2}}$, (2.3-5)

$\tan\phi = \text{tn}u = x(1-x^2)^{\frac{1}{2}}$, (2.3-6)

and

$K = F(k, \frac{\pi}{2})$ is the complete elliptic integral. (2.3-7)

The solution of (2.3-1) in terms of elliptic integrals is as follows: Write $v=dy/dt$ and (2.3-2) becomes

$$v\frac{dv}{dy} = -(ay + by^3), \tag{2.3-8}$$

so

$$\int_0^v v\,dv = -\int_{y_0}^{y} (ay + by^3)\, dy \tag{2.3-9}$$

and

$$v^2 = a(y_0^2 - y^2) + \tfrac{1}{2}b(y_0^4 - y^4). \tag{2.3-10}$$

Choosing the negative root,

$$v=dy/dt= -a^{\frac{1}{2}}(y_0^2 - y^2)^{\frac{1}{2}}[1+(b/2a)(y_0^2 + y^2)]^{\frac{1}{2}} \tag{2.3-11}$$

and therefore

$$t=-a^{\frac{1}{2}} \int_{y0}^{y} dw/(y_0^2 - w^2)^{\frac{1}{2}}[1+(b/2a)(y_0^2 + w^2)]^{\frac{1}{2}} \quad (2.3\text{-}12)$$

letting $w=y_0\cos\psi$, we have

$$t=a^{\frac{1}{2}}\int_0^{\varphi} d\psi/[1+(b/2a)y_0^2(1+\cos^2\psi)]^{\frac{1}{2}}, \quad (2.3\text{-}13)$$

with $\cos\varphi=y/y_0$, or $\varphi=\cos^{-1}(y/y_0)$. Thus if $\lambda^2=by_0^2/2(a+by_0^2)$, (2.3-13) may be written

$$t=(a+by_0^2)^{-\frac{1}{2}} \int_0^{\varphi} d\psi/[1-\lambda^2\sin^2\psi]^{\frac{1}{2}}. \quad (2.3\text{-}14)$$

Aside from the external multiplier, the right-hand side of (2.3-14) is an incomplete elliptic integral of the first kind with modulus λ. Thus in the notation from above, we have

$$t=(a+by_0^2)^{-\frac{1}{2}} F(\lambda,\varphi), \quad (2.3\text{-}15)$$

where

$$u=F(\lambda,\varphi) = \int_0^{\varphi} d\psi/[1-\lambda^2\sin^2\psi]^{\frac{1}{2}}. \quad (2.3\text{-}16)$$

By definition, sn$u$ = sinφ, where sn$u$ is the sine type of Jacobian elliptic function.

The solution of the equation (2.3-1) in terms of Jacobian elliptic functions will become useful when we address the two-core nonlinear coherent coupler.

Chapter 3: NLCC Optical Amplifier

Section 3.1: Introduction

The nonlinear coherent coupler (NLCC) has received much attention in the literature since its introduction in 1980[5]. As discussed above, the NLCC utilizes the coherent interaction of two optical waveguides placed in close proximity. If one disregards all nonlinear considerations, analysis shows that the waveguides periodically exchange power in a simple sinusoidal pattern. When the nonlinearities of the materials are taken into account, so that the amplitudes of the modes propagating affect the local index of refraction, there is a 'detuning' induced between the propagating waves, and coupling ceases to be sinusoidal. As the power levels increase, the associated nonlinearity and detuning increase. Complete coupling takes longer and longer (more distance propagated), and after a certain power threshold, complete coupling ceases to occur. When the NLCC is operated near this threshold between complete coupling occurring (below the threshold) and not occurring (above the threshold), very small changes in the input amplitudes can cause large changes in the output amplitudes.

The two-core nonlinear coherent coupler can of course be excited with light propagating in both directions. Modes

propagating in opposite directions (counter-propagating modes) do couple with each other, but not as strongly as modes propagating in the same direction (co-propagating modes). As will be demonstrated, coupling between counter-propagating modes also has the characteristic that the coupling is amplitude-dependent yet phase-independent, that is, the coupling depends only upon the amplitude of the modes, and not the phase of the modes. The basic concept behind the two-core counter-propagating optical amplifier is to operate with two rightwards-propagating modes with amplitudes near the unstable point, and to have leftwards-propagating modes of small amplitude cause large changes in the rightwards propagating modes. It is therefore possible to have signals of very small amplitudes cause large changes in the outputs of the amplifier, essentially producing an optical transistor, with different gains ($\delta P_{out}/\delta P_{in}$) for different operating points. The operation of this device in this fashion has been verified via computer simulation, with gains up to 28 observed.

The advantages of such a device are several. First, and most importantly, the device is completely optical, with no reliance on the electro-optic effect, and thus has none of the bandwidth limitations associated with electronic components. This is an important factor as optical communication systems need higher and higher bandwidth capabilities. Second, as will be shown, the device is phase-independent. This limits

the device to amplifying signals in which the phase of the signal carries no information (which is almost entirely the case in optical communication systems). In return, this characteristic provides much design flexibility. Designers need not worry if a signal to be amplified has propagated one half of a wavelength further than another, since only the amplitudes, and not the phases, of the signals affect the output of the amplifiers.

Section 3.2: Two-Core Unidirectional NLCC

Before beginning discussion of the bi-directional case, further discussion of the unidirectional case is necessary. The solutions derived above for the propagation of modes in the two-coupled-waveguide system must be examined to yield the proper operating lengths for a bidirectional coupler. We wish to identify, in our normalized system, the lengths at which 50% or 100% power transfer have occurred, and at which the power has returned 50% and 100% to the original core. These lengths are the integer quarter-periods, i.e., T/4, T/2, 3T/4, and T, and are available from the complete elliptic function *K*.

Section 3.3: Two-Core Bidirectional NLCC

The equations which describe the propagation in the bidirectional NLCC are developed as a combination of 1) the nonlinear coupled mode equations developed in §2.1.6, which include self-phase modulation, and 2) a cross-phase modulation term to be developed here. The cross-phase modulation term represents the coupling between two modes propagating in the same waveguide in opposite directions in a temporally and spatially local region.

If we consider a waveguide with electromagnetic waves E_1 and E_3 propagating in opposite directions (see Figure 21), then the total field in the guide is given by

$$E_T=[E_1(z)e^{-j\beta_L z}+E_3(z)e^{-j\beta_L z}]e^{-j\omega t}. \qquad (3.3\text{-}1)$$

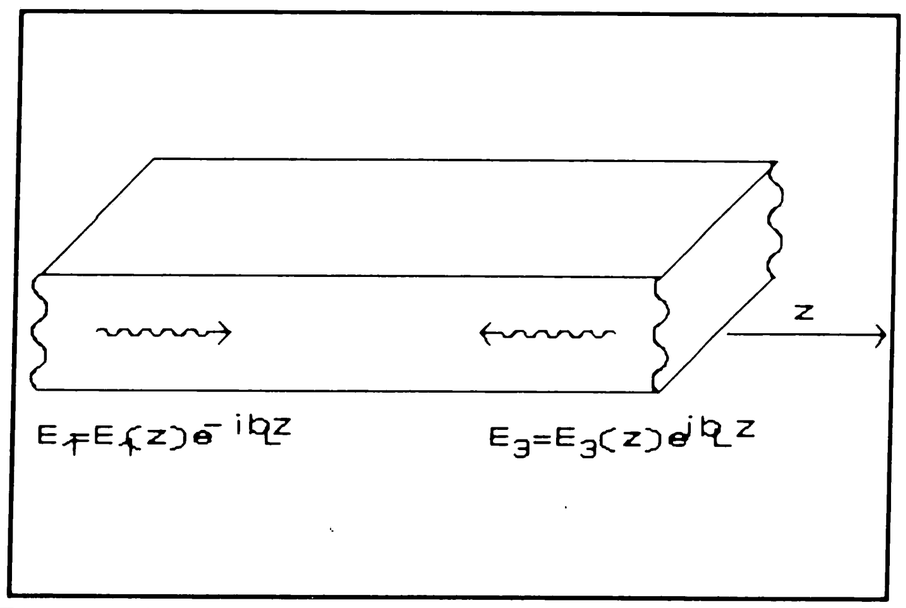

Figure 21: Waveguide with counterpropagating waves

The rightward-propagating wave has propagation constant $-\beta_L$ and the leftward-propagating wave has propagation constant $+\beta_L$. We then apply Maxwell's wave equation

$$\nabla^2 E + \frac{\omega^2 n^2}{c^2} E = 0,$$

remembering that for a non-linear material, $n=n_0 + In_2$, so $n^2=n_0^2 + 2n_0n_2|E_T|^2$, and also that the operator $\nabla^2 = \frac{\delta^2}{\delta z^2}$, yielding

$$\left[\ddot{E}_1 + 2j\beta_L\dot{E} - \beta_L^2E_1\right]e^{j\beta_Lz} + \left[\ddot{E}_3 - 2j\beta_L\dot{E}_3 - \beta_L^2E_3\right]e^{-j\beta_Lz}$$

$$+ \left[n_0^2 + 2n_0n_2|E_T|^2\right]\omega^2/c^2\left[E_1e^{j\beta_Lz} + E_3e^{-j\beta_Lz}\right] = 0. \quad (3.3\text{-}2)$$

Now, in (3.3-2), the $\ddot{E}_1$ and the $\ddot{E}_3$ can be neglected due to the standard slowly varying envelope approximation, and the $-\beta_L^2E_1$ and $-\beta_L^2E_3$ terms cancel with the n_0^2 in the third term, and we are left with

$$2j\beta_L\dot{E}_1e^{j\beta_Lz} - 2j\beta_L\dot{E}_3e^{-j\beta_Lz} +$$

$$\frac{2\omega^2n_0n_2}{c^2}\left[|E_1|^2 + |E_3|^2 + E_1E_3^*e^{2j\beta_Lz} + E_3E_1^*e^{-2j\beta_Lz}\right]$$

$$x\left[E_1e^{j\beta_Lz} + E_3e^{-j\beta_Lz}\right] = 0 \quad (3.3\text{-}3)$$

Gathering synchronous pieces (all terms with $e^{j\beta_Lz}$, $e^{-j\beta_Lz}$, $e^{2j\beta_Lz}$, $e^{-2j\beta_Lz}$), we have

$$2j\beta_L\dot{E}_1 + \frac{2\omega^2n_0n_2}{c^2}\left[|E_1|^2 + |E_3|^2 + |E_3|^2\right] = 0,$$

$$-2j\beta_L\dot{E}_1 + \frac{2\omega^2n_0n_2}{c^2}\left[|E_1|^2 + |E_3|^2 + |E_1|^2\right] = 0,$$

and therefore

$$j\dot{E}_1 + \frac{\omega n_2}{c}[\ |E_1|^2 + 2|E_3|^2\ ]E_1 = 0,$$
$$-j\dot{E}_3 + \frac{\omega n_2}{c}[\ |E_3|^2 + 2|E_1|^2\ ]E_3 = 0. \qquad (3.3\text{-}4)$$

From equations (3.3-4) we see the presence of two self-phase-modulation terms ($|E_1|^2$ and $|E_3|^2$) which represent the nonlinear interaction between the propagation of a mode and the index of refraction change it causes. We also see two cross-phase modulation terms ($2|E_3|^2$ and $2|E_1|^2$) which represent the interaction of a mode with a mode propagating the same velocity in the opposite direction in a spatially local region. A direct modification to the coupled mode equations (2.1.5-10) may then be made, yielding the bi-directional nonlinear coherent coupler equations

$$j\dot{E}_1(z) + \beta E_1(z) + \kappa E_2(z) + \frac{n_2\omega}{c}\left[|E_1(z)|^2 + 2|E_3(z)|^2\right]E_1(z)=0$$

$$j\dot{E}_2(z) + \beta E_2(z) + \kappa E_1(z) + \frac{n_2\omega}{c}\left[|E_2(z)|^2 + 2|E_4(z)|^2\right]E_2(z)=0. \qquad (3.3\text{-}5)$$

These equations describe mode propagation in a two-guide nonlinear coherent coupler with counterpropagating modes (see Figure 22).

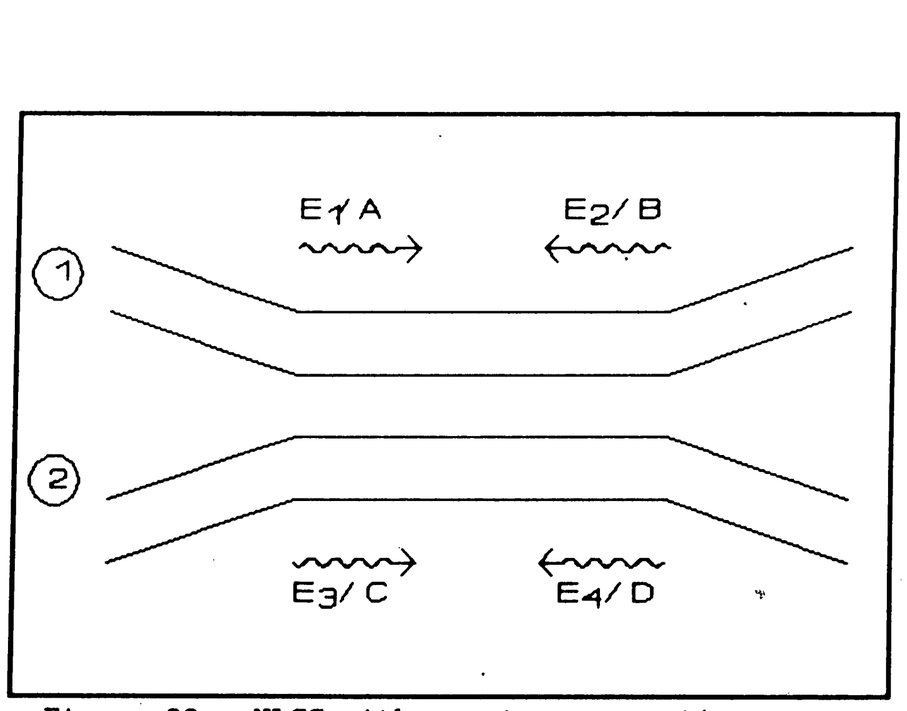

Figure 22: NLCC with counterpropagating waves

By the same method presented in §2.1.5 to verify that equations (2.1.5-10)

were functionally the same as equations (2.1.4-9), and using the normalization technique presented in §2.1.6, the normalized bi-directional NLCC equations may be written

$$j\dot{A} + \kappa B + [|A|^2 + 2|C|^2]A = 0$$
$$j\dot{B} + \kappa A + [|B|^2 + 2|D|^2]B = 0$$
$$-j\dot{C} + \kappa D + [|C|^2 + 2|A|^2]C = 0$$
$$-j\dot{D} + \kappa C + [|D|^2 + 2|B|^2]D = 0 \qquad (3.3\text{-}6)$$

where A is the z-dependence of the rightward propagating mode in guide 1, B is the z-dependence of the rightward propagating in guide 2, C is leftward propagating in guide 1, and D is leftward propagating in guide 2 (see Figure 22).

Coupling Coefficient κ

In general, the coupling coefficient κ is a complicated function involving the distance between the two waveguides, the surrounding index of refraction, the index of refraction in the waveguides, the propogation constants of the coupled modes, and the shapes of the mode tails in the guides. The integral (2.1.5-7) introduced in section 2.1.5, is a closed-form expression for the calculation of the coupling coefficient. It can be shown ([2]) that for two parallel identical channel waveguides, the coupling coefficient κ is given by

$$\kappa = \frac{2h^2 q e^{-qs}}{\beta W (q^2+h^2)}$$

(3.3-6)

where W is the channel width, s is the separation, h and β are the propagation constants in the y and z directions, respictively, and q is the extinction coefficient in the y direction.

Section 3.4: Computer Simulation of Bi-Directional NLCC

The equations derived above which describe the bi-directional NLCC case were next simulated using a digital computer. Equations (3.3-6) were separated into their real and imaginary components, yielding a boundary value ordinary nonlinear differential system of 8 equations in 8 unknowns. The following quantities were defined:

$$y_1(\eta) = \mathrm{Re}(A(\eta)),\ y_2(\eta) = \mathrm{Im}(A(\eta)),$$
$$y_3(\eta) = \mathrm{Re}(B(\eta)),\ y_4(\eta) = \mathrm{Im}(B(\eta)),$$
$$y_5(\eta) = \mathrm{Re}(C(\eta)),\ y_6(\eta) = \mathrm{Im}(C(\eta)),$$
$$y_7(\eta) = \mathrm{Re}(D(\eta)),\ y_8(\eta) = \mathrm{Im}(D(\eta)). \qquad (3.4\text{-}1)$$

By plugging these definitions into equations (3.3-6), the following system of 8 ordinary nonlinear differential equations was generated:

$$\dot{y}_1 = -y_4 - y_2(y_1^2 + y_2^2 + 2y_5^2 + 2y_6^2)$$
$$\dot{y}_2 = y_3 + y_1(y_1^2 + y_2^2 + 2y_5^2 + 2y_6^2)$$
$$\dot{y}_3 = -y_2 - y_4(y_3^2 + y_4^2 + 2y_7^2 + 2y_8^2)$$
$$\dot{y}_4 = y_1 + y_3(y_3^2 + y_4^2 + 2y_7^2 + 2y_8^2)$$
$$\dot{y}_5 = y_8 + y_6(y_5^2 + y_6^2 + 2y_1^2 + 2y_2^2)$$

$$\dot{y}_6 = -y_7 - y_5(y_5^2 + y_6^2 + 2y_1^2 + 2y_2^2)$$

$$\dot{y}_7 = y_6 + y_8(y_7^2 + y_8^2 + 2y_3^2 + 2y_4^2)$$

$$\dot{y}_8 = -y_5 - y_7(y_7^2 + y_8^2 + 2y_3^2 + 2y_4^2). \qquad (3.4\text{-}2)$$

To use the bi-directional NLCC as an optical amplifier, as discussed earlier, we must choose an 'operating point' of the amplifier somewhere near its unstable region. As the reader may recall, the unstable region in our normalized system, as developed above, is when the total power in the system is close to 2.0. Therefore, if we select an operating point characterized by rightward (or leftward) propagating power of magnitude close to 2.0, initially injected into one guide, and choose a length L of the coupler to ensure that at the right (or left) end of the coupler, the output of one guide is nominally zero, and the output of the other guide is equal to the input power, then any perturbations introduced propagating in a leftward (or rightward) direction will cause large variations in the output conditions. The physical description of the operation of the amplifier is modeled by the following initial boundary conditions. Assuming that power is initially injected into guide 1 in figure 22, then $A(\eta=0) = P_{in}$. Therefore, $y_1(0) = \mathrm{Re}(P_{in})$ and $y_2(0) = \mathrm{Im}(P_{in})$. Since no power is injected into guide 2 at the left end, we have $B(0)=0$, which tells us that $y_3(0) = 0$ and $y_4(0) = 0$. The length L of the coupler is then derived by the Jacobian

elliptic functions which describe the (uni-directional) propagation in the NLCC. At the right end of the coupler, we measure the outputs A(L) or B(L). At the right end of the coupler, we also introduce the perturbation power, P_{gate}. This takes the form of conditions on C(L) or D(L), depending upon where we choose to inject P_{gate}, which in turn place conditions upon $y_5(L)$ and $y_6(L)$ or $y_7(L)$ and $y_8(L)$. If we choose to inject P_{gate} into C, and inject 0 into D, then $y_7(L)=y_8(L) = 0$, and $y_5(L) = Re(P_{gate})$ and $y_6(L)=Im(P_{gate})$. So, for any given input power P_{in}, and any given power P_{gate}, we can place a total of 8 boundary conditions upon the problem, 4 on each end.

The numerical solution of this system involved several attempts before success was attained. The first attempt was to implement the solution using a finite-difference method known as the Adams-Gear method in Fortran IV on a Cyber 850 mainframe computer. The IMSL version 10 [16] software library was used to attempt a solution. The software succeeded when the leftward propagating power, P_{gate}, was zero (this is no longer solving a boundary value problem, but merely an initial value problem), but not for any non-zero values of P_{gate}.

Then a special method was devised using the Runge-Kutta initial value problem algorithm to successfully solve the system for all but the most unstable power levels. It was observed from the equations (3.3-6) that the rightward propagating waves coupled mainly with each other (through the

κA and κB terms). The coupling with the leftward-propagating waves, although important, was numerically much smaller. So it was proposed that a fourth-order Runge-Kutta method be used to solve the system from left to right, given the 4 initial conditions provided for the left side. Then, taking the 4 initial conditions on the left side, the Runge-Kutta method was used to solve the system from right to left. This procedure was continued back and forth until the system converged to a solution (see Flowchart, Figure 23).

With $P_{in} = 1.9 + j0$, and $P_{gate}=0.0 + j0$, we can calculate $\lambda=|P_{in}|^2/4.0 = 0.9025$ (from the methods discussed in §2.1.6). Thus the length L required for the power to completely couple into guide 2 and back into guide A is $4K(\lambda)$, where $K(\lambda)$ is the

```
1) Solving from   0.0000 to   4.5830
2) With  50 steps.
3) A(0)=  1.90 +  0.00j
4) B(0)=  0.00 +  0.00j
5) C(L)=   .05 +  0.00j
6) D(L)=  0.00 +  0.00j
7) Tolerance for NAG routine= .10E-07
8) Tolerance for convergence criteria.10E-07
9) Go...
10) Quit...
11) Clear matrix...
12) Max Iterations =  50
13) Graph the last one
14) Menu On/Off
15) Print Intermediate Outputs on/off (now 0)

Enter a number:
? 9
Start out with
A(0)=3.609999999999985 B(0)=0.000000000000000 C(0)=0.000000000000000 D(0)=0.000000000000000
A(L)=3.610000001513143 B(L)= .000000000000000 C(L)= .002500000000000 D(L)=0.000000000000000
Power=3.612500000073 deviation=1.479316863798E-8 its= 6
End up with
A(0)=3.609999999999985 B(0)=0.000000000000000 C(0)= .001480930728096 D(0)= .001019069344783
A(L)=3.609863528161483 B(L)= .000136473505047 C(L)= .002500000000000 D(L)=0.000000000000000
```

Figure 24: Computer Output for A(0)=1.0+j0.0, C(L)=0.05+j0.0

well-tabulated complete elliptic integral. In this case, the length L=4.5830. We choose n=50 points between η=0 and η=4.5830. For P_{gate}=0.0+j0.0, the algorithm described above obviously requires only 1 iteration to converge to an answer, i.e. one sweep from left to right. For P_{gate} = 0.05 + j0.0, we have $y_5(4.5830)=0.05$, $y_6(4.5830)=y_7(4.5830)=y_8(4.5830)=0.0$. After 6 iterations, the algorithm described above converges to a solution, and $|B(L)|^2$, the power emerging from guide 2, has changed from 0.0 to 1.36×10^{-4}. Thus in this case, the power gain was P_{out}/P_{in} = 0.0544. (See computer output, Figure 24.)

The Bi-directional case was explored at many P_{in}s and P_{gate}s, for many different lengths. We do not necessarily have to choose the length L=4$K(\lambda)$. If we choose a length L=2$K(\lambda)$, then the power injected into guide 1 has exactly coupled into guide 2, and at this length the output (rightwards-propagating at the right end in Figure 22) is measured from guide 1.

If we choose a length L=(2n+1)$K(\lambda)$, then exactly half of the power injected into guide 1 has coupled into guide 2, and half remains in guide 1. We may measure the output from either guide at this length. The P_{gate} will cause equal and opposite perturbations in each of these outputs. The output signal will thus be an amplified (or attenuated) version of the input signal, superimposed upon a constant component. This is the obvious disadvantage of choosing this length for

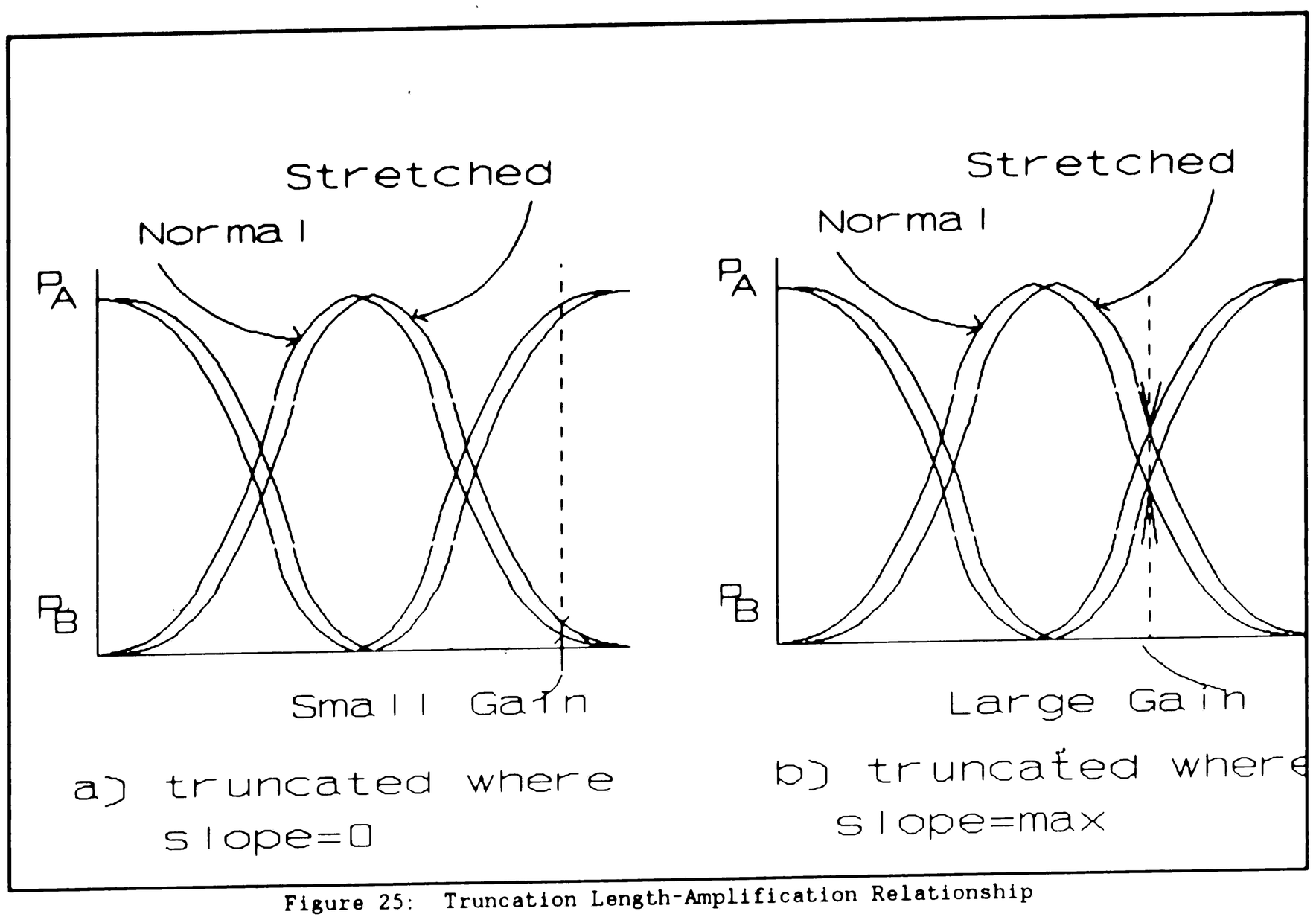

Figure 25: Truncation Length-Amplification Relationship

an amplifier. There is, however, an advantage. The lengths $L=(2n+1)K(\lambda)$, where half of the power is in each guide, provide higher amplification. The reasoning for this is as follows: when a gate signal is introduced into the system, is raises the total net power in the system, thus increasing any coupling lengths. This has the effect of stretching the coupling patterns. Obviously, a coupling pattern which is truncated at a point of higher slope of the coupling pattern will change more rapidly when 'stretched' than a pattern truncated at a point of low slope (see Figure 25). This results in higher amplification factors for amplifiers of length $(2n+1)K(\lambda)$, with the disadvantage being the associated

constant component in the output. As will be discussed in the conclusion, there are methods to cancel out this component of the signal in practical systems.

The Runge-Kutta algorithm described above solved most, but not all, cases. The cases which it was not able to solve (which would not converge) remain unsolved. But, the results available suggest that the proposed optical amplifier indeed has potential as a practical device.

Section 3.5: Results

Many simulations of the optical amplifier proposed were conducted. Not all of the cases simulated converged, and since it is not entirely possible to know if a solution will converge or not (in general, the closer the total injected power was to 2.0, the less the chance of convergence), some computer time was spent on solutions which did not converge. But the solutions which *did* converge produced some very encouraging results. Figure 26 lists the results for each of the 48 cases studied. Each row in the table represents a certain P_{in}, length (the n in the table is multiples of $K(\lambda)$ for that P_{in}), and P_{gate} input position, either guide C or D. Each column represents a different value of P_{gate}. The entries in the table are the power gains achieved for the particular configurations. Where the entries are not present, the gains

P_{in}	n	CD	2.50^{-3}	1.00^{-2}	2.25^{-2}	4.00^{-2}	6.25^{-2}	9.00^{-2}	1.23^{-1}	1.60^{-1}	2.03^{-1}	2.50^{-1}
1.60	1	C	4.20^{-1}	4.22^{-1}	4.24^{-1}	4.28^{-1}	4.32^{-1}	4.38^{-1}	4.44^{-1}	4.52^{-1}	4.60^{-1}	4.70^{-1}
1.60	2	C	9.54^{-4}	3.89^{-3}	8.59^{-3}	1.49^{-2}	2.27^{-2}	3.16^{-2}	4.15^{-2}	5.22^{-2}	6.33^{-2}	7.49^{-2}
1.60	3	C	1.16	1.15	1.14	1.14	1.13	1.13	1.14	1.16	1.21	1.30
1.60	4	C	8.99^{-4}	3.66-3	8.44^{-3}	1.55^{-2}	2.50^{-2}					
1.70	1	C	6.04^{-1}	6.06^{-1}	6.10^{-1}	6.15^{-1}	6.21^{-1}	6.29^{-1}	6.38^{-1}	6.49^{-1}	6.61^{-1}	6.74^{-1}
1.70	2	C	2.48^{-3}	9.54^{-3}	2.08^{-2}	3.54^{-2}	5.25^{-2}	7.14^{-2}	9.12^{-2}	1.12^{-1}	1.32^{-1}	
1.70	3	C	1.58	1.59	1.61	1.63	1.65	1.68	1.70	1.71	1.70	1.67
1.70	4	C	6.44^{-2}	2.32^{-1}	4.47^{-1}	6.62^{-1}	8.55^{-1}	1.02				
1.75	4	C	1.81^{-1}	6.65^{-1}	1.30	1.93	2.47	2.91	3.23	3.44	3.53	3.50
1.775	4	C	2.56^{-1}	9.56^{-1}	1.89	2.83	3.63	4.29	4.78	5.07	5.15	5.01
1.80	1	C	9.04^{-1}	9.08^{-1}	9.13^{-1}	9.21^{-1}	9.32^{-1}	9.44^{-1}	9.59^{-1}	9.77^{-1}	9.97^{-1}	1.02
1.80	2	C	6.39^{-3}	2.46^{-2}	5.23^{-2}	8.65^{-2}	1.24^{-1}	1.62^{-1}	2.00^{-1}			
1.80	3	C	3.24	3.31	3.46	3.72	4.16	4.91	5.84	6.06	5.61	
1.80	4	C	3.15^{-1}	1.20	2.42	3.65	4.75	5.73	6.54	7.03	7.09	6.81
1.80	6	C	9.73^{-3}	4.61^{-2}	1.57^{-1}	7.00^{-1}						
1.80	8	C	1.12	4.36	9.93	1.32^{+1}						

P_{in}	n	CD	2.50^{-3}	1.00^{-2}	2.25^{-2}	4.00^{-2}	6.25^{-2}	9.00^{-2}	1.23^{-1}	1.60^{-1}	2.03^{-1}	2.50^{-1}
1.80	10	C	9.06^{-2}	2.43^{-1}	3.09^{-1}	2.80^{-1}						
1.80	12	C	2.55	9.68	1.59^{+1}	4.00^{-2}	2.05^{+1}					
1.80	14	C	6.66^{-1}	4.19	9.53							
1.80	16	C	3.42	1.27^{+1}	2.87^{+1}							
1.825	4	C	3.17^{-1}	1.24	2.54	3.91	5.25	6.75	8.35	9.07	8.96	8.49
1.85	10	C	9.40^{-1}	2.75	3.39							
1.85	12	C	3.39^{-1}	9.35^{-1}	1.04							
1.85	14	C	5.22	1.79^{+1}								
1.85	16	C	4.32^{-1}	1.58	1.87							
1.85	1	C	1.14	1.14	1.15	1.16	1.18	1.20	1.22	1.24	1.27	1.30
1.85	1	D	1.13	1.13	1.12	1.11	1.10	1.08	1.06	1.04	1.01	9.87^{-1}
1.85	2	C	9.82^{-3}	3.77^{-2}	2.25^{-2}	1.30^{-1}	6.25^{-2}	2.36^{-1}				
1.85	2	D	1.01^{-2}	4.22^{-2}	1.02^{-1}	2.01^{-1}	3.57^{-1}	5.90^{-1}	9.02^{-1}	1.26	1.63	1.97
1.85	3	C	1.04	1.02	1.00	9.82^{-1}	6.25^{-2}	9.68^{-1}	1.08	8.43		
1.85	3	D	1.05	1.06	1.09	1.14	1.21	1.34	1.57	2.38	7.87	
1.85	4	C	2.21^{-1}	8.78^{-1}	1.86	2.93	4.05	5.76	9.89	1.07^{+1}	1.01^{+1}	9.35

P_{in}	n	CD	2.50^{-3}	1.00^{-2}	2.25^{-2}	4.00^{-2}	6.25^{-2}	9.00^{-2}	1.23^{-1}	1.60^{-1}	2.03^{-1}	2.50^{-1}
1.85	4	D	2.17^{-1}	8.20^{-1}	1.54	1.98						
1.85	5	C	1.70^{+1}	1.73^{+1}	1.63^{+1}	1.38^{+1}						
1.85	5	D	1.65^{+1}	1.55^{+1}	1.35^{+1}							
1.85	6	C	4.02^{-1}	1.67	3.60	4.49						
1.85	6	D	3.96^{-1}	1.60	4.31	1.10^{+1}						
1.85	7	C	4.12	3.58	3.01	2.53	2.13					
1.85	7	D	4.63	5.85	1.18^{+1}	4.00^{-2}	2.14^{+1}					
1.85	8	C	1.08	4.42	8.00							
1.85	8	D	1.04	4.03	1.02^{+1}	4.00^{-2}	1.47^{+1}	1.37^{+1}				
1.90	1	C	1.48	1.49	1.50	1.52	1.55	1.58	1.62	1.66	1.71	1.77
1.90	1	D	1.48	1.47	1.46	1.44	1.41	1.39	1.36	1.32	1.29	1.25
1.90	2	C	1.16^{-2}	4.51^{-2}	9.57^{-2}	1.58^{-1}	2.25^{-1}					
1.90	2	D	1.19^{-2}	4.99^{-2}	1.20^{-1}	2.33^{-1}	4.03^{-1}	6.40^{-1}	9.25^{-1}	1.22	1.50	1.75
1.90	3	C	5.09	5.16	5.21	5.21	5.10			1.06^{+1}		
1.90	3	D	5.04	4.94	4.73	4.39	3.93					
1.90	4	C	5.46^{-2}	2.55^{-1}	7.87^{-1}	3.24				1.24^{+1}	1.07^{+1}	9.00
1.85	5	D	5.67							1.40^{+1}	1.20^{+1}	

configurations. Where the entries are not present, the gains could not be computed due to non-convergence.

As can be seen from the table, and as would be expected from having a knowledge of the equations which describe the system, the gain of the amplifier increases when the power P_{in} becomes close to the critical value of 2.0. As a rough estimate, as the difference between P_{in} and 2.0 halves, i.e. $(2.0 - P_{in}) \rightarrow (2.0 - P_{in})/2$, the gain doubles. The gain of the amplifier also increases as the length of the amplifier is increased. Choosing the odd multiples of $K(\lambda)$ for lengths of the amplifier increases the gain tremendously, at the expense of having a constant component of the output signal.

The optical amplifier proposed and existing electrical transistors are similar. First, both must be properly biased at a certain 'operating point'. For the optical transistor, this consists of choosing a P_{in} and an appropriate length, or vice versa, choosing a length and an appropriate P_{in}. Second, both exhibit gains which are dependent upon the operating point. The gains of the optical amplifier discussed in this thesis also depend upon the gate power, so instead of the output power depending linearly upon the gate power (as in an electrical transistor), there is a nonlinear relation between the gate and output powers in the optical transistor.

The graph in Figure 27 depicts the simulated values of gain versus P_{gate} for different values of P_{in}, different

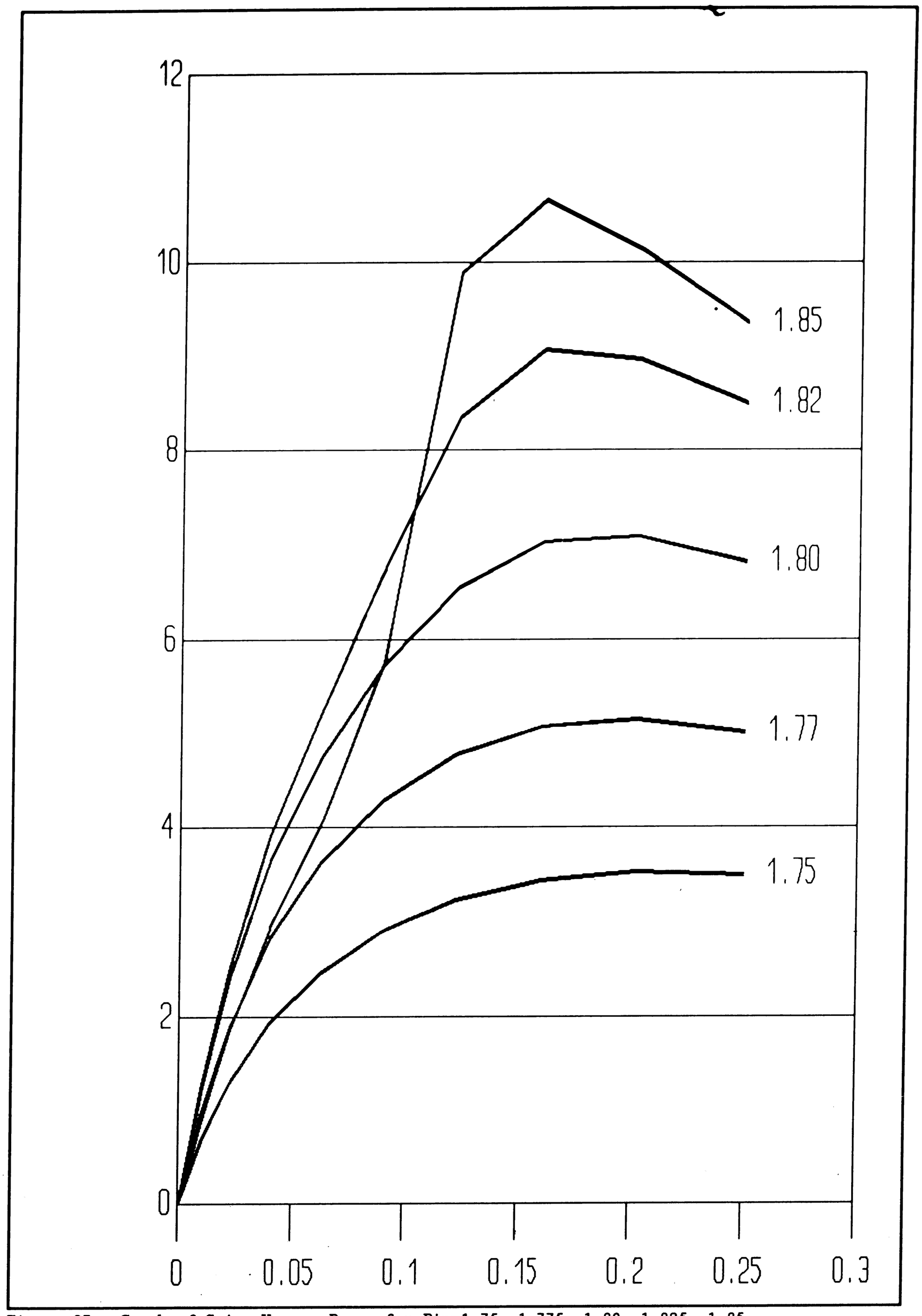

Figure 27: Graph of Gains Versus P_{gate} for Pin=1.75, 1.775, 1.80, 1.825, 1.85.

lengths, and different injection points for P_{gate}.

In view of these results, the optical amplifier proposed has very promising characteristics.

Chapter 4: Conclusion

The preceding thesis presented an examination of the operation of the proposed light amplifier. Amplifications of up to 29 were observed via computer simulation, with lower amplifications existing when P_{in} was far in value from the unstable point and higher amplifications present as P_{in} became closer to the unstable point. The limitation of the numerical technique in simulating the amplifier prevented simulation of situations even closer to the unstable "saddle" point of 2.0 in our normalized system, and it is assumed that even higher amplification regions exist when P_{in} is closer in value to the unstable point. Therefore, higher amplifications are assumed by this author to be possible, although computer simulation was not able to verify this assumption.

The inherent problem with increasing P_{in} closer and closer to the unstable point is that any fluctuations in P_{in} are more and more in evidence at the output. The design of a practical amplifier would have to take this "tradeoff" of higher amplification and higher P_{in} sensitivity versus lower amplification and lower P_{in} sensitivity into account.

The highest amplifications were also observed in situations when the length of the coupling region was such that at the output end of the amplifier, the signals had the highest "slope" (see figure 25). The disadvantage of this

amplifier length was that the output signal contained a constant component with the amplified signal superimposed upon it.

Further speculation on the implementation of the proposed amplifier, however, leads to a possible solution to both of these problems - high sensitiviy to P_{in} fluctuations and a constant component of the output signal. If it were possible to superimpose a signal on top of the output signal which was exactly equal in magnitude and opposite in phase from the constant part of the output signal, and if this signal were always equal and opposite from the constant component of the output signal, then both of these problems would be solved. A method has been speculated, using a beam-splitter, another two-core coupler, and a phase shifter (see figure 28). If the P_{in} which is injected into the left end of the amplifier is half of a beam which has been split, then the other half of the beam may be used to cancel out the P_{in} which remains at the right end of the amplifier. In figure 28, P_1 is split into two equal propogating beams, P_2 and P_{in}. In addition to traveling through a NLCC (NLCC #1 in figure 28), P_2 travels through a region in which an electric field may be

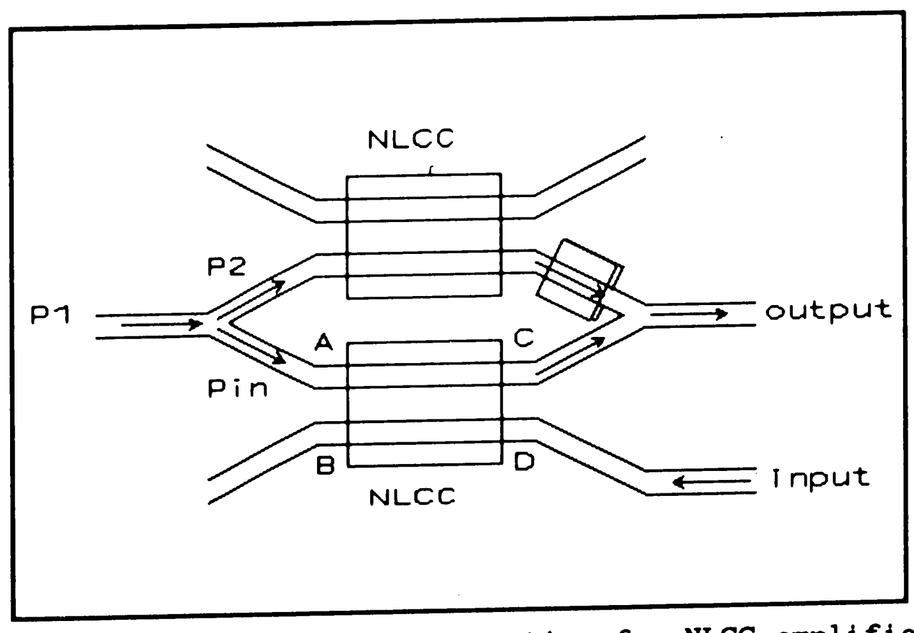

Figure 28: Possible configuration for NLCC amplifier

induced, and due to the electro-optic effect, a slight phase shift may be induced. In the nominal case, in which the (left-propagating) input at guide D is zero, P_2 and P_{in} propogate through two identical Nonlinear Coherent Couplers, and P_2 propogates through the electro-optic "fine tuning" region, and the beams recombine, (rightwards-propogating) at node C. If the voltage in the "fine tuning" region is adjusted properly, so that there is a 180° phase shift between P_2 and P_{in}, then the beams recombining cancel each other out, and the output is zero. This is true *regardless of fluctuations in* P_1, and therefore this scheme solves the problem of sensitivity to fluctuations in P_1.

Then whenever there is a signal P_{gate} introduced (leftward-propagating) at D, and it causes an (amplified) perturbation in the quantity of P_{in} emerging from C and recombining with P_2, it will cause an amplified deviation from zero in the amount of power emerging at P_{out}. This scheme thus removes any "constant" portion of the output signal, leaving only the amplified version of the input signal, thus solving the problem of the constant component of the output signal.

The issue of bandwidth is always of importance when considering the operation of amplifiers. In the derivations of the equations to be used in computer simulations of the

proposed amplifer, there was no allowance given for signals of different frequencies propogating. This thesis has, therefore, not examined the operation of the amplifier at different frequencies, and has no definite conclusions to draw about the bandwidth of the amplifier. It was discussed in §2.1.4 that the relaxation times for some nonlinear materials are on the order of 100fs, and it is postulated that this provides an upper limit on the frequencies of signals which may be effectively amplified by this device. The fact that the counter-propogating signals interact based only upon their amplitude, and not their phase (see § 3.3), provides (in this author's opinion) a strong argument for the frequency independence of this amplifier's operation. Further work must address this issue.

The results of this thesis have answered some questions and raised many more, as will any thorough treatment of a subject. The computer simulation of the operation of this device was a necessary first step in its development.

LIST OF REFERENCES

[1] Keiser, G. Optical Fiber Communications. New York: McGraw-Hill, 1983.

[2] Hunsperger, R. G. Integrated Optics: Theory and Technology. Second Edition. Springer Series in Optical Sciences, Volume 33. Berlin, Heidelberg, New York, Tokyo: Springer-Verlag, 1985.

[3] Friberg, S. R., and Smith, P. W., "Nonlinear Optical Glasses for Ultrafast Optical Switches" *IEEE J. Quantum Electron.*, Vol. QE-23 (1975), pp. 2089-2094.

[4] Thomazeau, I., Etchepare, J., Grillion, G., and Migus., A., "Electronic nonlinear optical susceptibilities of silicate glasses" *Opt. Lett.*, Vol. 10 (1985), pp. 223-225.

[5] Jensen, S. M. "The non-linear coherent coupler, a new optical logic device," presented as Conf. Integrated and Guided-Wave Optics, Incline Village, CA 1980.

[6] Jensen. S. M., "The Nonlinear Coherent Coupler" *IEEE J. Quantum Electron.*, Vol. QE-18 (1982), pp. 1580-1583.

[7] Friberg, S. R., Silberberg, Y., Oliver, M. K., Andrejco, M. J., Saifi, M. A., and Smith, P. W., "Ultrafast all-optical switching in a dual-core fiber nonlinear coupler" *Appl. Phys. Lett.*, Vol. 51 (1987), pp. 1135-1137.

[8] Halas, N. J., Kroekel, D., and Grischkowsky, D., "Ultrafast light-controlled optical-fiber modulator" *Appl. Phys. Lett.*, Vol. 30 (1987), pp. 886-888.

[9] Gusovskii, D. D., Dianov, E. M., Maier, A. A., Neustruev, V. B., Schlovskii, E. I., and Shcherbakov, I. A., "Nonlinear light transfer in tunnel-coupled optical waveguides" *Sov. J. Quantum Electron.*, Vol. 15 (1985), pp 1523-1526.

[10] Li Kam Wa, P., Sitch, J. E., Mason, N. J., Roberts, J. S., and Robson, P. N., "All Optical Multiple-Quantum-Well Waveguide Switch" *Electron. Lett.*, Vol 21 (1985), pp. 26-28.

[11] Jin, R., Chuang, C. L., Gibbs, H. M., Koch, S. W., Polky, J. N., and Pubanz, G. A., "Picosecond all-optical switching in single-mode GaAs/AlGaAs strip-loaded

nonlinear directional couplers" *Appl. Phys. Lett.*, Vol. 53 (1988), pp. 1791-1793.

[12] Kitayama, K., and Wang, S., "Optical pulse compression by nonlinear coupling" *Appl. Phys. Lett.*, Vol. 43 (1983), pp. 17-19.

[13] Carnahan, B., Luther, H. A., Wilkes, J. O. Applied Numerical Methods. New York: John Wiley & Sons, Inc., 1969.

[14] Greenhill, A. G. The Applications of Elliptic Functions. New York: Dover Publications Inc., 1959.

[15] McLachlan, N. W. Ordinary Non-Linear Differential Equations In Engineering And Physical Sciences. Oxford: Clarendon Press, 1950.

[16] IMSL Libraries, Volume 10. Houston, Texas: IMSL Incorporated, 1987.

[17] Winful, H. G., "Pulse Compression in Optical Fibers" *Appl. Phys. Lett.*, Vol. 46 (1985), pp. 527-529.

[18] Marcuvitz, N, Editor. Waveguide Handbook. Massachusetts Institute of Technology Radiation Laboratory Series. New York: McGraw Hill, 1951.

[19] Tamir, T., Editor. Integrated Optics. Topics In Applied Physics, Vol. 7. Berlin: Springer-Verlag, 1979.

[20] Lee, D. L. Electromagnetic Principles of Integrated Optics. New York: John Wiley & Sons, 1986.

[21] Snyder, A. W., and Love, J. D. Optical Waveguide Theory. New York: Chapman and Hall, 1983.

[22] Kull, M., and Manneberg, G., "Integrated Optical Amplifier for Fast Phase-Modulated Signals" *J. Lightwave Technol.*, Vol. 7 (1989), pp.331-335.

[23] Zenteno, L., "Group Delay Dispersion Measurements in InGaAsP 1.3-μm Optical Amplifiers" *J. Lightwave Technol.*, Vol. 7 (1989), pp. 39-44.

[24] Stegeman, G. I., and Seaton, C. T., "Nonlinear Integrated Optics" *J. Appl. Phys.*, Vol. 58 (1985), pp. R57-R78.

[25] Daino, B., Gregori, G., and Wabnitz, S., "Stability analysis of nonlinear coherent coupling" *J. Appl. Phys.*, Vol. 58 (1985), pp. 4512-4514.

[26] Milne-Thomson, L. M. Jacobian Elliptic Function Tables. New York: Dover Publications Inc., 1950.

[27] Hodgman, C. D., Editor in Chief. C. R. C. Standard Mathematical Tables. Cleveland, Ohio: Chemical Rubber Publishing Company, 1952.

[28] NaG Fortran Library Manual, Mark 12. Downers Grove, Illinois: Numerical Algorithms Group Limited, 1987.

Appendix: Computer Program Description and Notes

The computer program used to do the simulations discussed in this thesis was written in Fortran-77 on the Cyber 850 computer at Lehigh University. It was developed in the Programming Environment running under the NOS/VE operating system. It uses the Numerical Algorithms Group (NAG) Fortran library for calculation of the Runge-Kutta method.

When the program is run, a menu appears with 15 sets of parameters which the user may change simply by selecting the number of the parameter the user wishes to change. Each of the choices will be discussed:

1) Set left and right boundaries: When this item is selected, the user is prompted for the left and right boundaries for the solution. If the user enters positive numbers in response to these boundaries, the numbers will be multiplied by $K(\lambda)$, the quarter-period of oscillation of the NLCC for the currently selected A(0). If the user enters negative numbers, the numbers will be multiplied by -1 and used for the boundaries.

2) Set number of steps: The user is prompted to enter the total number of points to be solved for in the interval.

3), 4), 5), 6): Set boundary conditions: The user is prompted for the real and imaginary components of the respective boundary conditions A(0), B(0), C(L), D(L).

7) Tolerance for NAG routine: The user is prompted for a number to be passed to the NAG Runge-Kutta routine as the desired accuracy. Usually it is not necessary to change this from the default of 1×10^{-8}.

8) Tolerance for convergence criteria: The user is prompted for a number which is the tolerance for convergence of the matrix. After each iteration from right to left to right, the amount of change in this iteration is compared to the convergence tolerance to decide whether or not to do another iteration. Sometimes it is necessary to raise this number to 1×10^{-4}.

9) Go: Perform the simulation, iterating until convergence is reached as dictated by (8) or until the maximum number of iterations have been performed, as dictated by (12).

10) Quit: Ends the program.

11) Clear Matrix: Clears the matrix which contains all of the intermediate steps. Normally, this is not necessary,

and in fact, when operating near regions where convergence is slow, it is often better to start out with the matrix full of numbers from a previous nearby case.

12) Maximum Iterations: Sets the maximum number of iterations to be performed. If the program fails to converge in the prescribed number of iterations, it will exit with an appropriate message.

13) Graph the last one: Plots the last simulated case on the screen. To plot this simulated graph to the plotter, quit the program (10), and use the NOS/VE command PLOT.

14) Menu On/Off: Toggles a variable which turns the printing of the menu on and off. The default is ON, and when running the program from a batch file is it often convenient to switch the menu off.

15) Print Intermediate Outputs On/Off: Toggles a variable which tells the program whether or not all of the intermediate points are to be printed at the conclusion of each simulation.

A hard copy and a disk file of this program are in the posession of Dr. Nikolai Eberhardt.

Vita: Christopher Milner

Christopher James Milner was born in Chicago, Illinois, on October 10, 1966. After attending high school in West Windsor, New Jersey, he attended Lehigh University in Bethlehem, Pennslyvania, and recieved a Bachelor of Science in Computer Engineering in June, 1987. He then continued studies at Lehigh University and will receive the degree of Master of Science in Electrical Engineeering in June, 1989. His thesis work was in the field of integrated optics; specifically, he performed computer verification of the operation of a new optical amplification scheme. He plans to pursue a professional position in the field of integrated optics.

Mr. Milner is a member of Tau Beta Pi and Eta Kappa Nu.